Cell Reports

Article

Residue Y362 is crucial for $FLIP_L$ to impart catalytic activity to pro-caspase-8 to suppress necroptosis

Graphical abstract

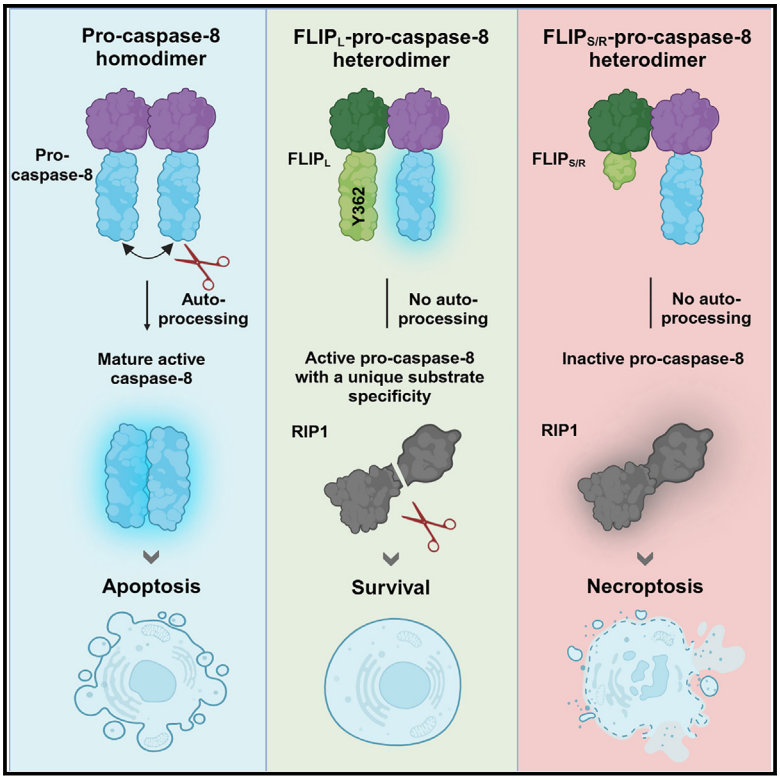

Highlights

- Intact $FLIP_L$ and pro-caspase-8 are required for $FLIP_L$-pro-caspase-8 heterodimer's function
- Evolving to Y from C at 362 residue of $FLIP_L$ is crucial for pro-caspase-8 to cleave RIP1
- Residue Y362 is crucial for $FLIP_L$ to suppress necroptosis in cells and mice

Authors

Mao Hong, Xiurong Wu, Peng He, ..., Yingying Zhang, Jiahuai Han, Zhang-Hua Yang

Correspondence

y.zhang@xmu.edu.cn (Y.Z.), jhan@xmu.edu.cn (J.H.), zhanghuayang@zju.edu.cn (Z.-H.Y.)

In brief

Pro-caspase-8 heterodimerizes with $FLIP_L$ to build up the important checkpoint of necroptosis, but the molecular mechanism is not fully understood. Hong et al. show that Y362 in the protease-like domain of $FLIP_L$ holds it in a special structure to impart pro-caspase-8 unique catalytic activity toward RIP1 to prevent necroptosis.

Hong et al., 2024, Cell Reports *43*, 114966
November 26, 2024
https://doi.org/10.1016/j.celrep.2024.114966

CellPress

Cell Reports

CellPress
OPEN ACCESS

Article

Residue Y362 is crucial for FLIP$_L$ to impart catalytic activity to pro-caspase-8 to suppress necroptosis

Mao Hong,[1,5] Xiurong Wu,[3,5] Peng He,[1] Rangxin Peng,[1] Lang Li,[1] Su-Qin Wu,[4] Jianbang Zhao,[1] Aidong Han,[1] Yingying Zhang,[1,*] Jiahuai Han,[1,4,*] and Zhang-Hua Yang[2,6,*]

[1]State Key Laboratory of Cellular Stress Biology, School of Life Sciences, Faculty of Medicine and Life Sciences, Xiamen University, Xiamen, Fujian 361102, China

[2]Department of Gastroenterology, Sir Run Run Shaw Hospital, Zhejiang University School of Medicine, Zhejiang University, Hangzhou, Zhejiang 310012, China

[3]Zhejiang Provincial Key Laboratory of Pancreatic Disease, MOE Joint International Research Laboratory of Pancreatic Diseases, The First Affiliated Hospital, Zhejiang University School of Medicine, Zhejiang University, Hangzhou, Zhejiang 310012, China

[4]Laboratory Animal Center, Xiamen University, Xiamen, Fujian 361102, China

[5]These authors contributed equally

[6]Lead contact

*Correspondence: y.zhang@xmu.edu.cn (Y.Z.), jhan@xmu.edu.cn (J.H.), zhanghuayang@zju.edu.cn (Z.-H.Y.)

https://doi.org/10.1016/j.celrep.2024.114966

SUMMARY

The pro-form of caspase-8 prevents necroptosis by functioning in a proteolytically active complex with its catalytic-dead homolog, FLICE (FADD [Fas-associated death domain]-like interleukin 1β-converting enzyme)-like inhibitory protein long-form (FLIP$_L$). However, how FLIP$_L$ imparts caspase-8 the catalytic activity to suppress necroptosis remains elusive. Here, we show that the protease-like domain of FLIP$_L$ is essential for the activity of the caspase-8-FLIP$_L$ heterodimer in blocking necroptosis. While substitution of two amino acids whose difference may contribute to the pseudo-caspase property of FLIP$_L$ with the corresponding amino acids in caspase-8 does not restore the protease activity of FLIP$_L$, one of the amino acid replacements, tyrosine (Y) 362 to cysteine (C), is sufficient to completely abolish the activity of the caspase-8-FLIP$_L$ heterodimer in cleaving receptor-interacting protein 1 (RIP1), thus releasing the necroptosis blockade. Unconstrained necroptosis is observed in embryonic day (E)10.5–E11.5 embryos of FLIP$_L$-Y362C knockin mice. Collectively, these results reveal that the protease-like domain of FLIP$_L$ has a special structure that imparts the pro-caspase-8-FLIP$_L$ heterodimer a unique catalytic activity toward RIP1 to prevent necroptosis.

INTRODUCTION

Apoptosis and necroptosis are two types of programmed deaths. Both can be induced by tumor necrosis factor alpha (TNF-α).[1] Upon TNF-TNF receptor 1 (TNFR1)engagement, complex I is formed with TRADD (TNFR1-associated death domain protein), RIP1 (receptor-interacting protein 1), TRAF2, cIAP1/2, and LUBAC (linear ubiquitin chain assembly complex). Ubiquitinated RIP1 in complex I is responsible for inflammatory signaling pathways such as nuclear factor κB (NF-κB) activation, and the deubiquitination of RIP1 switches the signal to cell death pathways.[2–6] When RIP1 is deubiquitylated, complex II (also called the death-inducing signaling complex [DISC]) containing RIP1, caspase-8 (C8), and FADD is formed instead to initiate caspase cascade and subsequent apoptotic cell death.[7–10] The necrosome that contains RIP3 and mixed-lineage kinase-like protein (MLKL) could be formed to initiate necroptosis when caspase-8 activity is compromised.[11–16] MLKL interacts with RIP3 in the necrosome, undergoes phosphorylation, and translocates onto the plasma membrane to execute necroptosis.[17–22]

Induction of necroptosis is regulated at multiple levels, among which the blockade checkpoint by pro-caspase-8 is an essential one, as evidenced by numerous reports on cells and genetic studies in mice.[1,23,24] The inactivation of pro-caspase-8 artificially by a caspase inhibitor is often required for the initiation of necroptosis,[25,26] and a few necroptosis-competent cells (like L929 cells) restrict caspase-8 activity naturally by p90 ribosomal s6 kinase (RSK)-mediated phosphorylation.[27] Disruption of caspase-8 blockade can result in the embryonic lethality of mice, which can be fully rescued by the ablation of RIP3 or MLKL.[28–31] It is pro-caspase-8, not the matured caspase-8, that is responsible for the suppression of necroptosis.[29,32] Small interfering RNA (siRNA) knockdown experiments showed that the ability of pro-caspase-8 to inhibit necroptosis requires the expression of FLICE-like inhibitory protein long-form (FLIP$_L$), a catalytically inactive caspase-8 homolog.[29]

FLIP (also known as cFLIP) in humans is encoded by the *CFLAR* gene, which is composed of 14 exons, resulting in a few splicing variants. FLIP$_L$, the long isoform of FLIP, is a 55 kDa protein containing two N-terminal DEDs (death effector recruitment domains) and a C-terminal caspase-like domain, which highly resembles the

structure of pro-caspase-8.[33,34] All splicing variants of FLIP are believed to form heterodimers with pro-caspase-8 via DED-DED interactions.[33–36] An assumption was that all FLIP isoforms inhibit the activation of caspase-8 through heterodimerization, as overexpression of either the short or long isoform of FLIP can block pro-caspase-8 processing, leading to decreased apoptosis.[37–41] However, the forced dimerization of $FLIP_L$ with pro-caspase-8 showed that $FLIP_L$ was able to activate full-length pro-caspase-8 toward a special substrate specificity that can efficiently cleave local substrates, including RIP1.[29,42–46] Short forms of FLIP, through heterodimerization with pro-caspase-8, also blocked pro-caspase-8 processing but failed to impart pro-caspase-8 activity toward RIP1.[35,45,46] In the absence of FLIP, both apoptosis and necroptosis could be executed.[29,36,47–52] It is clear that only $FLIP_L$, not FLIP short forms or pro-caspase-8, can impart pro-caspase-8 specific activity to cleave RIP1. However, how $FLIP_L$, through dimerization with pro-caspase-8, enables it to suppress necroptosis remains elusive.

In this article, we showed that the ability of $FLIP_L$ to impart special activity to pro-caspase-8 requires its structural integrity. The change of a single residue, Y362 (tyrosine 362), an evolutionarily conserved amino acid in the protease-like (PL) domain of $FLIP_L$, to the corresponding amino acid C362 (cysteine 362) in pro-caspase-8 abolished this function of $FLIP_L$. Despite losing its ability to convey pro-caspase-8 for RIP1 cleavage, the Y362-to-Cys mutation in $FLIP_L$ retains its inhibitory effect on pro-caspase-8 processing. We further validated the importance of $FLIP_L$-Y362-mediated caspase-8 activation *in vivo* by generating $FLIP_L$-Y362C knockin mutant mice. Mutation of Y362 of $FLIP_L$ caused unconstrained embryonic lethality in mice, with an even stronger necroptotic signal than what was observed in the mice with an uncleavable RIP1 D325A mutation.[53–56] Thus, our study demonstrated the importance of the pseudo-protease domain and the requirement of Y362 in that domain in cooperation with pro-caspase-8 to specifically suppress necroptosis and shed light on the coevolution of $FLIP_L$ and caspase-8 in the regulation of necroptosis.

RESULTS

Genetic deletion confirms that $FLIP_L$ is required for pro-caspase-8 to suppress TNF-induced necroptosis

L929 cells are murine fibrosarcoma cells that can undergo necroptosis upon TNF stimulation, and the necroptosis could be strongly enhanced by pan-caspase inhibitor benzyloxycarbonyl-Val-Ala-Asp-fluoromethylketone (zVAD).[57,58] A previous study showed the indispensable role of $FLIP_L$ in preventing RIP3-dependent necroptosis by siRNA-mediated knockdown of $FLIP_L$ in cells.[29] To elucidate the molecular mechanism by which $FLIP_L$ collaborates with caspase-8 to control necroptosis, we generated *Cflar* knockout (*Cflar* KO), *Casp8* KO, and *Casp8*, *Cflar* double KO (*Casp8*, *Cflar* DKO) L929 cells (Figure S1A). In mice, the *Cflar* gene encodes two protein isoforms, designated as $FLIP_L$ (FLIP long form) and $FLIP_R$ (FLIP short form) due to alternative splicing.[34] We checked the FLIP expression profile in L929 cells and found that only $FLIP_L$ exists (Figure S1A).

As expected, deletion of either *Casp8* or *Cflar* sensitized L929 cells to TNF-induced cell death (Figure 1A). Unlike *Casp8* KO L929 cells that died in typical necrotic morphology (Figure S1B), *Cflar* KO cells died in both apoptotic and necrotic morphologies (Figure S1B). Consistently, both apoptosis (caspase-8 activation) and necroptosis markers (p-RIP3) were strongly increased in these cells (Figures 1B and S1C). The cell death in *Cflar* KO L929 cells could be partially prevented by either the caspase-3 inhibitor DEVD or the RIP1 inhibitor Necrostatin-1 (Nec-1) alone but was completely prevented when DEVD and Nec-1 were used in combination (Figure S1D). Collectively, these data confirmed that $FLIP_L$ inhibits both apoptosis and necroptosis.

To assess the role of $FLIP_L$ in suppressing necroptosis, we generated *Casp8*, *Cflar* DKO L929 cells, which, as anticipated, behaved the same as *Casp8* KO L929 cells upon TNF stimulation (Figures 1A, 1C, and S1B). We reconstituted *Casp8*, *Cflar* DKO L929 cells with pro-caspase-8 and $FLIP_L$ alone or in combination (Figure S1E) and took the phosphorylation of RIP3/MLKL as a marker of necroptosis induction. As Figures 1D–1F show, expression of neither pro-caspase-8 nor $FLIP_L$ alone was able to dampen TNF-induced necroptosis. In contrast, the expression of $FLIP_L$ together with pro-caspase-8 completely blocks TNF-induced necroptosis (Figures 1D–1F). Thus, $FLIP_L$ partners with pro-caspase-8 to block TNF-induced necroptosis.

The integrity of both $FLIP_L$ and pro-caspase-8 is required for the suppression of TNF-induced necroptosis

We next sought to figure out how $FLIP_L$ activates pro-caspase-8 to suppress TNF-induced necroptosis. The same as pro-caspase-8, $FLIP_L$ is composed of two DED domains (DED1 and DED2) followed by a PL domain.[33,34] We constructed truncated $FLIP_L$ mutants, $FLIP_L$ without one or both of the DED domains ($FLIP_L$ ΔDED), or $FLIP_L$ without a PL domain ($FLIP_L$ ΔPL) (Figure 2A) and expressed these $FLIP_L$ truncates into *Cflar* KO L929 cells. We found that compared to wild-type $FLIP_L$ (WT-$FLIP_L$), these truncated $FLIP_L$ mutants could not enable pro-caspase-8 to inhibit necroptosis (Figure 2B). These data indicated that both the DED domains and PL domain were required for $FLIP_L$ to synergize with pro-caspase-8 on necroptosis suppression. As DED domains were reported to be required for the recruitment of $FLIP_L$ and pro-caspase-8 to their adaptors, such as FADD,[35,36,59] we proposed that DED domains are required for complex formation, and the PL domain in $FLIP_L$ is likely to be responsible for function together with pro-caspase-8 in inhibiting necroptosis.

We then generated catalytic inactive pro-caspase-8 (C362S), uncleavable pro-caspase-8 (DDAA) (Figure 2C), and reconstituted their expression with or without $FLIP_L$ co-expression in *Casp8*, *Cflar* DKO L929 cells. The data showed that the inhibitory effect of $FLIP_L$-synergized pro-caspase-8 on necroptosis requires catalytic active pro-caspase-8 in its uncleaved form (Figures 2D–2G). Thus, our data demonstrated that both $FLIP_L$ and pro-caspase-8 is required in its intact form for the suppression of TNF-induced necroptosis.

Residue Y362 in the PL domain of $FLIP_L$ is crucial for its synergy with pro-caspase-8 to suppress necroptosis

$FLIP_L$ and pro-caspase-8 shall evolve from the same ancestor based on their structural similarity (Figures 2A, 2C, S2A, and S2B). The protease activity has been lost in $FLIP_L$,[33,34,47] which is consistent with the fact that some of the residues crucial for

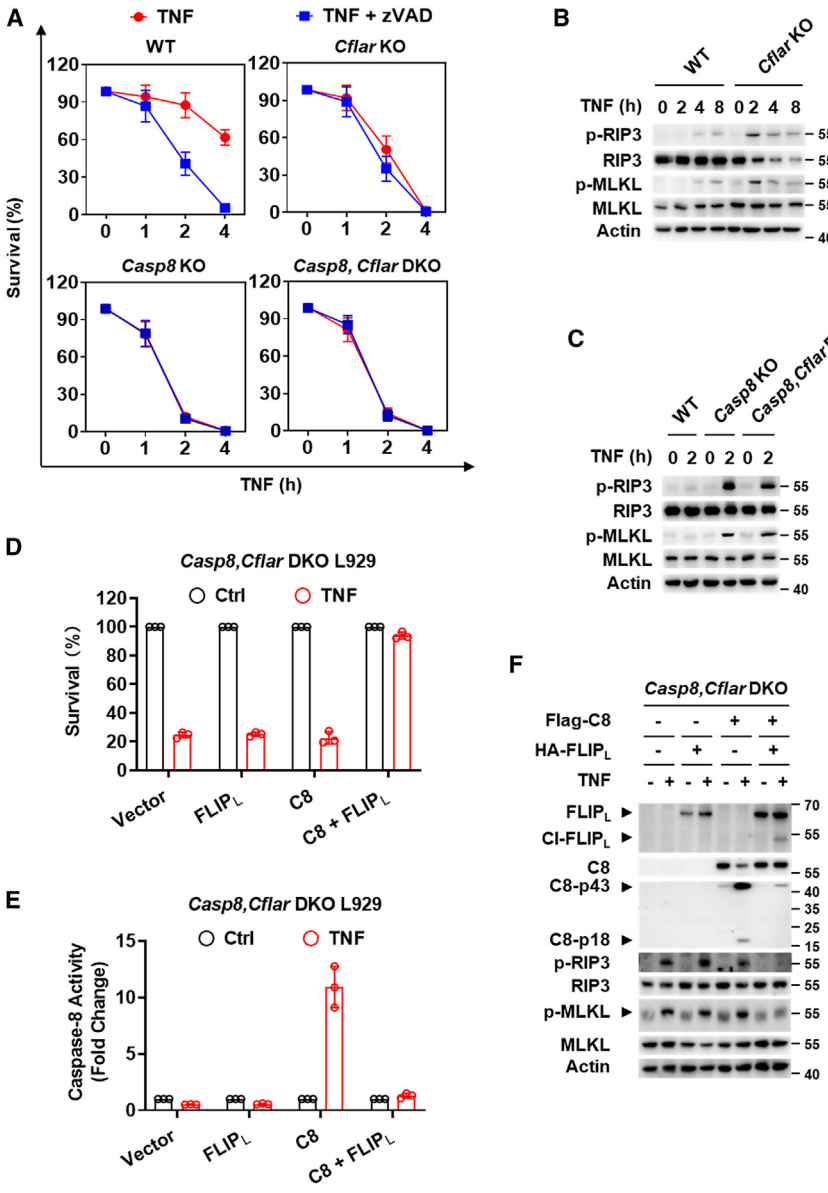

Figure 1. FLIP$_L$ is required for pro-C8 to suppress TNF-induced necroptosis

(A) Wild-type (WT), *Cflar* knockout (KO), *Casp8* KO, and *Casp8*, *Cflar* double KO (DKO) L929 cells were treated with TNF (10 ng/mL) or TNF+zVAD (20 μM) for different periods of time as indicated. The cell viabilities were measured. Data are presented as means ± SDs of three independent experiments.

(B) WT and *Cflar* KO L929 cells were treated with TNF for different periods as indicated. The cell lysates were analyzed by immunoblotting to detect phosphoproteins and proteins as indicated. p-RIP3, phospho-RIP3; p-MLKL, phospho-MLKL.

(C) WT, *Casp8* KO, and *Casp8*, *Cflar* DKO L929 cells were treated with TNF for different periods as indicated. The cell lysates were analyzed by immunoblotting to detect phosphoproteins and proteins as indicated.

(D–F) *Casp8*, *Cflar* DKO L929 cells reconstituted with caspase-8 (C8) and FLIP$_L$ alone or in combination were treated with TNF for 2 h. The cell viabilities (D) and C8 activity (E) were measured. Data are presented as means ± SDs of three independent experiments. The cell lysates were analyzed by immunoblotting to detect phosphoproteins and proteins as indicated (F).

All results are representative of at least two independent experiments. See also Figure S1.

protease activity in caspase-8 are not present in FLIP$_L$. In mice, H319, G320, and C362 of caspase-8 are involved in catalysis and R262, Q360, R415, and T421 of caspase-8 are involved in the formation of the binding pocket for the carboxylate side chain of P1 Asp (Figure S2A).[60] The *Cflar* gene appears to arise from tandem duplication events of the ancestral *casp8* gene after the divergence of vertebrates (Figure S2C).[61–63] Sequence alignment revealed that the amino acid sequences between the protease domain of caspase-8 and the PL domain of FLIP$_L$ are highly conserved, but the two residues H319 and C362, essential for catalysis in caspase-8, are changed to L317 and Y362 in FLIP$_L$ (Figure S2A). These amino acid substitutions are worth a detailed study.

Because only the FLIP$_L$-caspase-8 heterodimer but not the pro-caspase-8 homodimer inhibits necroptosis,[29] we speculated that FLIP$_L$ has acquired a unique function that directs pro-caspase-8 to suppress necroptosis. To test this possibility, we mutated L317 and Y362 in FLIP$_L$ to His and Cys(L317H+Y362C). By expressing this mutant into *Cflar* KO L929 cells (Figure S3A), we found that FLIP$_L$(L317H+Y362C) completely lost the ability to synergize with pro-caspase-8 to suppress necroptosis, while it retained the ability to prevent the processing of pro-caspase-8 (Figures 3A–3C). Consistently, we found that FLIP$_L$(L317H+Y362C) lost the ability to disrupt RIP1-RIP3 necrosome formation (Figure 3D). Co-immunoprecipitation showed that FLIP$_L$(L317H+Y362C) interacted with pro-caspase-8 like FLIP$_L$(WT) did (Figure S3B), indicating that the defect of FLIP$_L$(L317H+Y362C) in suppressing necroptosis is not due to the failure of FLIP$_L$-pro-caspase-8 hetero-interactions. When these two residues were mutated to their corresponding residues in caspase-8 individually, FLIP$_L$(L317H) retained the ability to suppress necroptosis, while FLIP$_L$(Y362C) lost this ability (Figure 3E). Thus, the Y362C single-residue mutation in FLIP$_L$ abrogates its necroptosis suppression function.

Previous studies have shown that the overexpression of FLIP$_L$ in HeLa cells could induce apoptosis and that the residue Y360 (in humans, corresponding to Y362 in mice) was important for this function, as the substitution of Y360 with Phe (phenylalanine) disrupted the function of FLIP$_L$ in apoptosis.[64] Therefore, in addition to mutating Y362 of FLIP$_L$ to Cys, we also mutated Y362 to

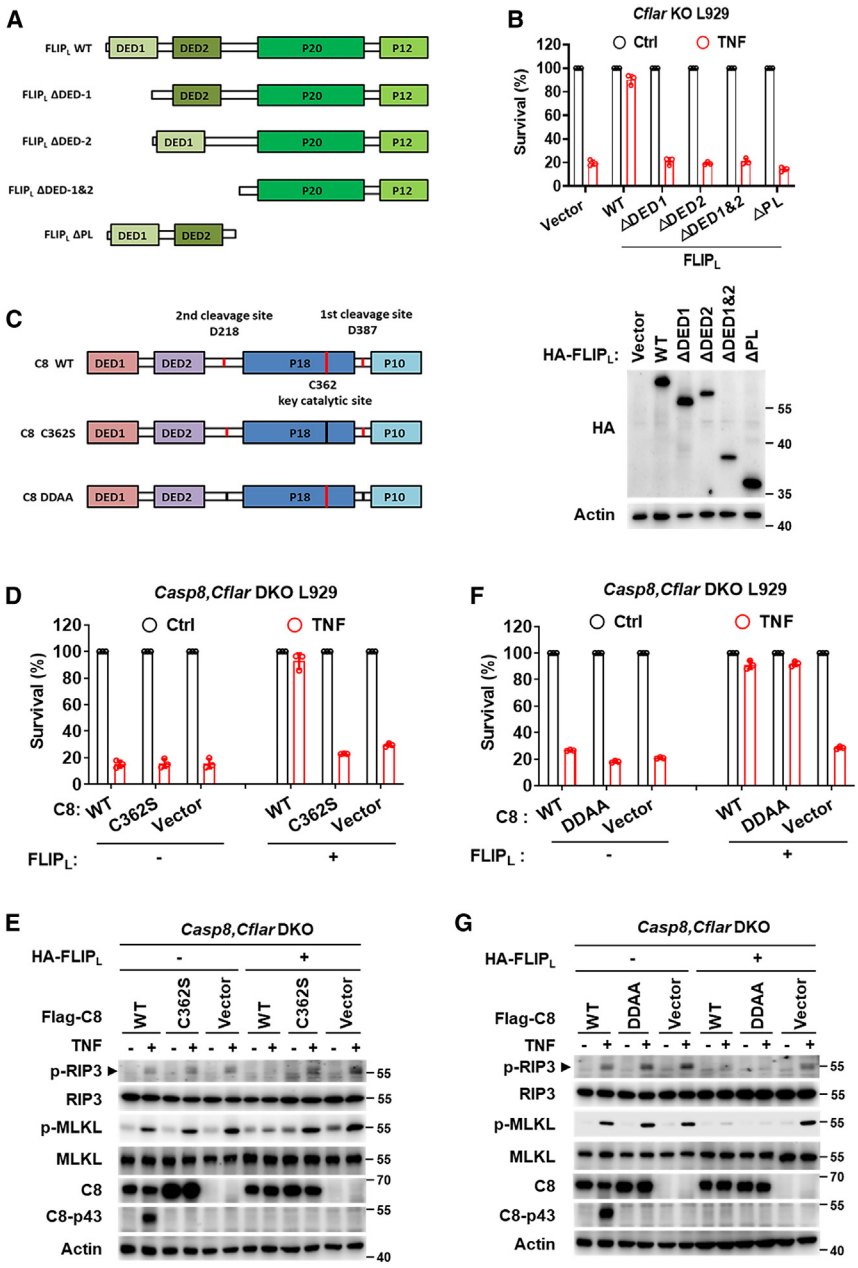

Figure 2. The integrity of both FLIP$_L$ and pro-C8 is required for the suppression of TNF-induced necroptosis

(A) Schematic diagram of truncated FLIP$_L$ mutants. FLIP$_L$ ΔDED, FLIP$_L$ without DED domains; FLIP$_L$ ΔPL, FLIP$_L$ without a protease-like (PL) domain.

(B) *Cflar* KO L929 cells reconstituted with hemagglutinin (HA)-FLIP$_L$ WT/ΔDED/ΔPL were treated with TNF for 2 h. The cell viabilities were measured. Data are presented as means ± SDs of three independent experiments. The protein expression level is analyzed by immunoblotting.

(C) Schematic diagram of C8 mutants. C8 C362S, catalytically inactive C8 mutant; C8 DDAA, uncleavable C8 mutant; DDAA, D218A+D387A.

(D and E) *Casp8*, *Cflar* DKO L929 cells reconstituted with FLAG-C8 WT/C362S in the absence or presence of HA-FLIP$_L$ were treated with TNF for 2 h. The cell viabilities were measured (D). Data are presented as means ± SDs of three independent experiments. The cell lysates were analyzed by immunoblotting as indicated (E).

(F and G) *Casp8*, *Cflar* DKO L929 cells reconstituted with FLAG-C8 WT/DDAA in the absence or presence of HA-FLIP$_L$ were treated with TNF for 2 h. The cell viabilities were measured (F). Data are presented as means ± SDs of three independent experiments. The cell lysates were analyzed by immunoblotting as indicated (G).

All results are representative of at least two independent experiments.

Phe to analyze Y362F's effect. By expressing these two FLIP$_L$ mutants into *Cflar* KO L929 cells, we found that both FLIP$_L$(Y362F) and FLIP$_L$(Y362C) functioned the same as WT-FLIP$_L$ in inhibiting the activation of caspase-8 (Figures 3E and 3F). In contrast, only FLIP$_L$ with Y362C but not Y362F lost the ability to suppress TNF-induced necroptosis (Figures 3E and 3F). Co-immunoprecipitation experiments showed that both FLIP$_L$(Y362F) and FLIP$_L$(Y362C) interacted with pro-caspase-8 (Figure 3G). Collectively, our data demonstrated that residue Y362 is crucial for FLIP$_L$ to suppress necroptosis.

The specific activity of the FLIP$_L$-pro-caspase-8 heterodimer toward RIP1 is largely affected by the structure near the Y362 in FLIP$_L$. The loss of function by specifically mutating Y362 to Cys but not Phe may explain, in part, why the pro-caspase-8 homodimer cannot suppress necroptosis, as one of the proteins in the dimer cannot have a Cys at this position. We then tested the effect of substituting C362 in caspase-8 with tyrosine (Y), the corresponding residue in FLIP$_L$. By reconstitution of WT caspase-8 (C8-WT) and C362Y-mutated caspase-8 (C8-C362Y) (Figures S3C–S3E), we found that the C362Y mutation completely abolished the catalytic activity of caspase-8. However, the C362Y mutation in caspase-8 could not render it as FLIP$_L$, as it failed to synergize with C8-WT to block necroptosis (Figure S3E). Besides, the mutation of Y362 to Cys in FLIP$_L$ had no impact on either the oligomerization of FLIP$_L$ (Figure S3F) or its protein half-life when reconstituted in *Cflar* KO L929 cells (Figure S3G).

Structural analyses of the loss-of-function mutant (Y362C) and no-effect mutant (Y362F) of FLIP$_L$

We then compared the structural differences between the caspase-8 homodimer and the FLIP$_L$-caspase-8 heterodimer. Structural superposition of the human caspase-8 homodimer (PDB: 6PX9)[65] and FLIP$_L$-caspase-8 heterodimer (PDB: 3H11)[44] reveals significant structural differences between the

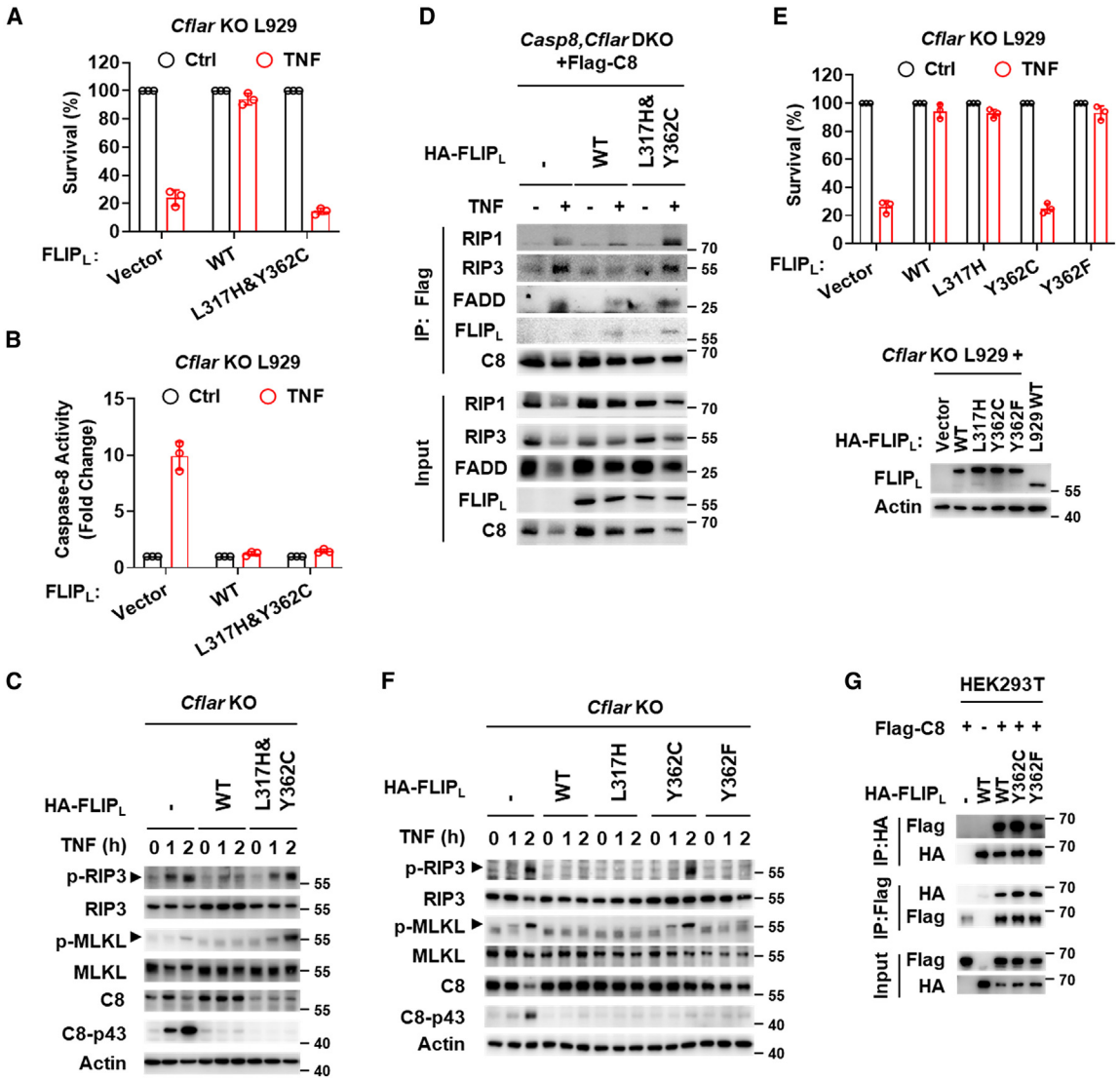

Figure 3. Residue Y362 in the protease-like domain of FLIP$_L$ is crucial for its synergizing with pro-C8 to suppress necroptosis

(A and B) *Cflar* KO L929 cells reconstituted with HA-FLIP$_L$ WT or mutants were treated with TNF for 2 h. The cell viabilities (A) and caspase-8 (C8) activity (B) were measured. Data are presented as means ± SDs of three independent experiments.

(C) The same cells as in (A) and (B) were treated with TNF for different periods of time as indicated. The cell lysates were analyzed by immunoblotting as indicated.

(D) *Casp8*, *Cflar* DKO L929 cells reconstituted with FLAG-C8 WT and HA-FLIP$_L$ WT or mutant were treated with TNF for 2 h. Then, immunoprecipitation with anti-FLAG antibody was performed in these cells. The cell lysates and immunoprecipitates were analyzed by immunoblotting as indicated.

(E) *Cflar* KO L929 cells reconstituted with HA-FLIP$_L$ WT/its mutants as indicated were treated with TNF for 2 h. The cell viabilities were measured. Data are presented as means ± SDs of three independent experiments.

(F) The same cells as in (E) were treated with TNF for different periods of time as indicated. The cell lysates were analyzed by immunoblotting as indicated.

(G) HEK293T cells were transfected with FLAG-C8 and HA-FLIP$_L$ WT/its mutants as indicated. Immunoprecipitation with anti-FLAG antibody or anti-HA antibody was performed in these cells 24 h post-transfection. The cell lysates and immunoprecipitates were analyzed by immunoblotting as indicated.

All results are representative of at least two independent experiments. See also Figures S2 and S3.

FLIP$_L$-p12 and caspase-8B subunits (Figures S4A–S4D). The two β-turn regions of caspase-8 located at residues N407-W420 (T1 region) and N452-K461 (T2 region) are disordered in the structure of the caspase-8 homodimer, whereas these corresponding regions in FLIP$_L$ are well ordered in the FLIP$_L$-caspase-8 heterodimer structure (Figure S4C). Structural analysis indicates that residue Y360 (corresponding to Y362 in murine FLIP$_L$) of FLIP$_L$-p43 is involved in stabilizing the T1 and T2 regions of FLIP$_L$-p12 (Figure S4D).

To better explore why cystine cannot be retained in FLIP$_L$ for its function, we generated a structural model of the mouse FLIP$_L$-caspase-8 heterodimer using AlphaFold 3.0.[66] Superposition of the mouse FLIP$_L$-caspase-8 heterodimers to their human homologs (PDB: 3H11) showed remarkably high structural similarity

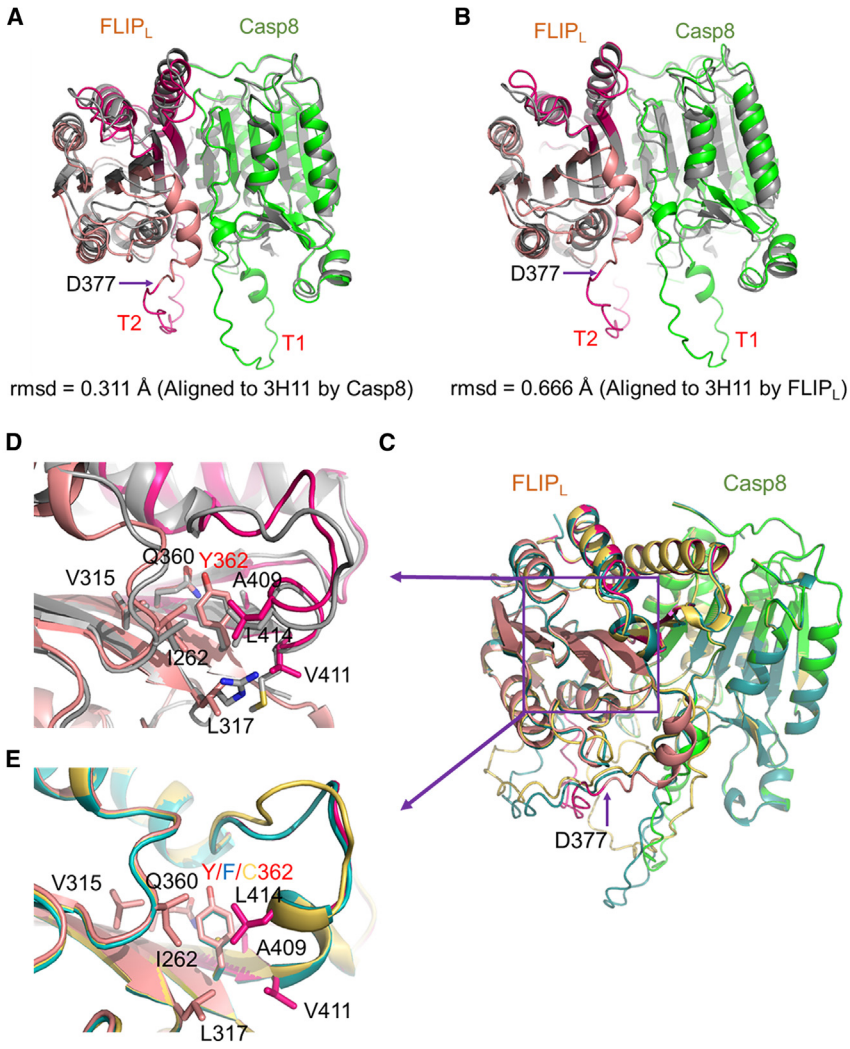

Figure 4. Structural analysis of mouse FLIP$_L$-caspase-8 heterodimer

(A and B) Structural superposition of mouse FLIP$_L$-caspase-8 heterodimer to their human homologs (PDB: 3H11) using alignments of caspase-8 (A) and FLIP$_L$ (B). The structural model of the mouse FLIP$_L$-caspase-8 heterodimer was predicted by AlphaFold 3.0. The C-terminal FLIP$_L$ cleaved at D377 corresponding to D376 of its human homolog is colored in magenta. The structure of the human homologs is colored in gray.

(C–E) Structural superposition of mouse FLIP$_L$-caspase-8 heterodimer with mutations Y362F (cyan) and Y362C (yellow). The structural models of the mouse FLIP$_L$-caspase-8 heterodimer with mutations were predicted by AlphaFold 3.0 and aligned to their WT. The overall alignment (C, RMSD: ~0.2 Å) and the sticks show the key residues surrounding Y362 with hydrophobic interactions (D and E). The C-terminal FLIP$_L$ cleaved at D377 corresponding to D376 of its human homolog is colored in magenta. The crystal structure of the human homologs is colored in gray (D).

See also Figure S4.

(root-mean-square deviation [RMSD]: 0.3–0.7) when alignments were performed using each component (Figures 4A and 4B). We also produced the structural models of mouse FLIP$_L$-caspase-8 heterodimer with Y362F and Y362C using AlphaFold 3.0, which are well aligned with their human homologs (PDB: 3H11) when using FLIP$_L$ as an anchor (RMSD: 0.2; Figure 4C). Further analyses of FLIP$_L$-Y362 showed that the tyrosine residue mediates a wide hydrophobic interaction network with I262, V315, L317, Q360, A409, V411, and L414 (Figure 4D). The Y362F mutant does not affect any hydrophobic interactions with these key residues in its pocket, but Y362C eliminates most of these due to the lack of a benzene ring (Figure 4E). This suggests that the preservation of the local structure in FLIP$_L$ is essential for the proper function of the FLIP$_L$-pro-caspase-8 heterodimer.

The basic structure of the PL domain in FLIP$_L$ is important for its function of imparting pro-caspase-8 with anti-necroptosis activity

We mentioned earlier that in addition to H319, G320, and C362, which are critical for protease activity, R262, Q360, R415, and T421 of caspase-8 are essential in the formation of the binding pocket (Figure S2A).[60] FLIP$_L$ lacks the amino acid corresponding to R262 in caspase-8, and G320, Q360, R415, and T421 are conserved in FLIP$_L$. To evaluate whether the basic structure of the PL domain in FLIP$_L$ is involved in the blockade of necroptosis, we mutated each of these four conserved amino acids or all of them together to alanine (A) in FLIP$_L$. The four single amino acid mutants of FLIP$_L$ behaved the same as those of WT-FLIP$_L$ in imparting pro-caspase-8 anti-necroptosis activity (Figure 5A). However, when the four amino acids were all mutated (4A mutation), FLIP$_L$ lost its ability to impart pro-caspase-8 anti-necroptosis activity (Figures 5B and 5D) but retained its ability to inhibit auto-processing of pro-caspase-8 (Figures 5C and 5D). Collectively, our data indicated that not only is the FLIP$_L$-specific site Y362 essential for the function of FLIP$_L$ but the basic protease-domain structure in FLIP$_L$ is also required to impart the anti-necroptosis function to pro-caspase-8.

Residue Y362 of FLIP$_L$ is crucial for FLIP$_L$-pro-caspase-8 heterodimer-mediated RIP1 cleavage

Previous studies showed that in a cell-free system, the FLIP$_L$-pro-caspase-8 heterodimer displayed the ability to cleave RIP1.[42] Since the cleavage of RIP1 is required for the suppression of TNF-induced necroptosis,[53–55,67] we assessed the role of FLIP$_L$ in synergizing with pro-caspase-8 to cleave RIP1 in cells. By substituting the DED domains of pro-caspase-8 and FLIP$_L$ with the FKBP (FK506-binding protein)/FRB (FKB12 rapamycin binding) domains, respectively, we could use AP21967 to induce the formation of a heterodimer between

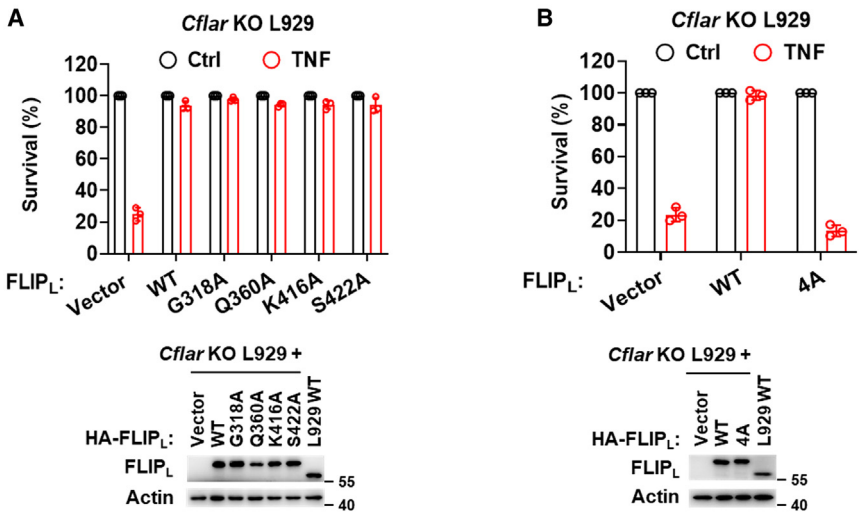

Figure 5. The basic structure of the protease-like domain in FLIP$_L$ is important for its function in imparting pro-caspase-8 the anti-necroptosis activity

(A) *Cflar* KO L929 cells reconstituted with HA-FLIP$_L$ WT or mutants were treated with TNF for 2 h. The cell viabilities were measured. Data are presented as means ± SDs of three independent experiments.

(B and C) *Cflar* KO L929 cells reconstituted with HA-FLIP$_L$ WT/4A mutants were treated with TNF for 2 h. The cell viabilities (B) and caspase-8 activity (C) were measured. Data are presented as means ± SDs of three independent experiments.

(D) The same cells as in (B) were treated with TNF for different periods of time as indicated. The cell lysates were analyzed by immunoblotting as indicated.

All results are representative of at least two independent experiments.

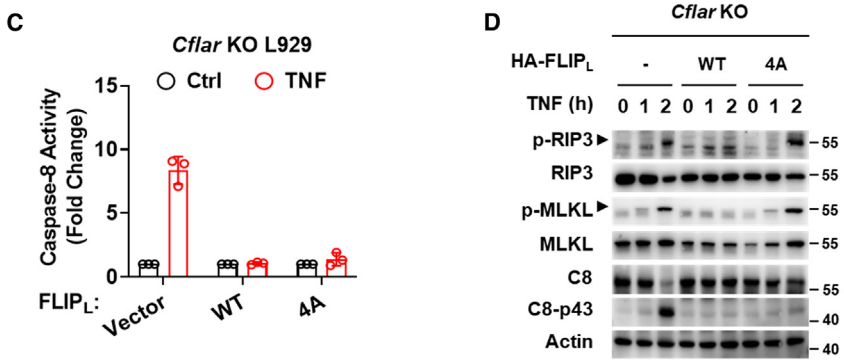

pro-caspase-8 and FLIP$_L$ specifically. We found that in 293T cells, the heterodimer of pro-caspase-8 with either FLIP$_L$(WT) or FLIP$_L$(Y362F) cleaved endogenous RIP1, but in contrast, the heterodimer of pro-caspase-8 with FLIP$_L$(Y362C) could not cut RIP1 (Figure 6A). To further determine the role of FLIP$_L$ in RIP1 cleavage during necroptosis progress, we also analyzed the RIP1 cleavage in TNF-induced necroptosis. To avoid the potential interference from the auto-processing of pro-caspase-8, we used non-cleavable pro-caspase-8 (DDAA) for the reconstitution of pro-caspase-8 expression. To avoid cell-death-caused sample loss that can interfere with the results of western blotting, we used *Casp8*, *Cflar*, *Rip3* triple KO (*Casp8*, *Cflar*, *Rip3* TKO) L929 cells, in which the reconstitution of pro-caspase-8 and FLIP$_L$ expression is not sufficient for necroptosis induction. In *Casp8*, *Cflar*, *Rip3* TKO L929 cells reconstituted with non-cleavable pro-caspase-8 (C8-DDAA) together with FLIP$_L$(WT) or FLIP$_L$(Y362C), we detected TNF-induced RIP1 cleavage in the cells expressing C8-DDAA and FLIP$_L$(WT) but not C8-DDAA plus FLIP$_L$(Y362C) (Figure 6B). We also performed experiments using *Casp8*, *Cflar* DKO L929 cells and included a reactive oxygen species (ROS) scavenger, butylated hydroxyanisole (BHA), in cell culture that can inhibit cell death via blocking ROS-mediated amplification loop.[68]

Consistent with the results obtained by using *Casp8*, *Cflar*, *Rip3* TKO L929 cells, FLIP$_L$(Y362C) cannot enable C8-DDAA to cleave RIP1 (Figure 6C). Collectively, these data suggest that after heterodimerization with pro-caspase-8, the Y362 residue is crucial for FLIP$_L$ to impart protease activity of pro-caspase-8 for the cleavage of RIP1.

Tyrosine residue at 362 of FLIP$_L$ is crucial for FLIP$_L$ to function in the embryonic development of mice

To validate the role of Y362 in FLIP$_L$ *in vivo*, we generated *Cflar* Y362 to Cys knockin mice, a mutant mouse bearing the Y362C mutation in FLIP$_L$ (Figure S5A). We first obtained *Cflar*$^{+/Y362C}$ mice, which were viable and showed no difference compared with *Cflar*$^{+/+}$ mice. When analyzing FLIP$_L$ protein expression levels in different tissues and primary cells from adult *Cflar*$^{+/Y362C}$ mice, we unexpectedly found that the protein expression level of FLIP$_L$ in *Cflar*$^{+/Y362C}$ mice was about half of that of WT in most of the samples tested (Figure S5B). We also compared the mRNA levels of FLIP between *Cflar*$^{+/Y362C}$ mice and *Cflar*$^{+/+}$ mice using bone marrow-derived macrophage (BMDM) samples and found that the FLIP mRNA levels in *Cflar*$^{+/Y362C}$ mice are comparable with those in *Cflar*$^{+/+}$ mice (Figure S5C). Although we did not observe any defect in the protein level of FLIP$_L$ in our cell-line-based experiments (Figure S3H), the Y362C mutation of FLIP$_L$ severely affected the protein level of FLIP$_L$ *in vivo* and in primary cells. Further breeding of *Cflar*$^{+/Y362C}$ mice did not result in the birth of any *Cflar*$^{Y362C/Y362C}$ mouse (Figure S5D). Thus, the Y362-to-C knockin mouse of FLIP is very likely the same as the *Cflar* KO mouse, which is embryonically lethal at around embryonic day (E)10.5–E11.5.[48,49]

Because of the lack of FLIP$_L$ protein, we would not distinguish whether the defect of the *Cflar*$^{Y362C/Y362C}$ mouse in embryo development resulted from no FLIP$_L$ protein or the loss function of

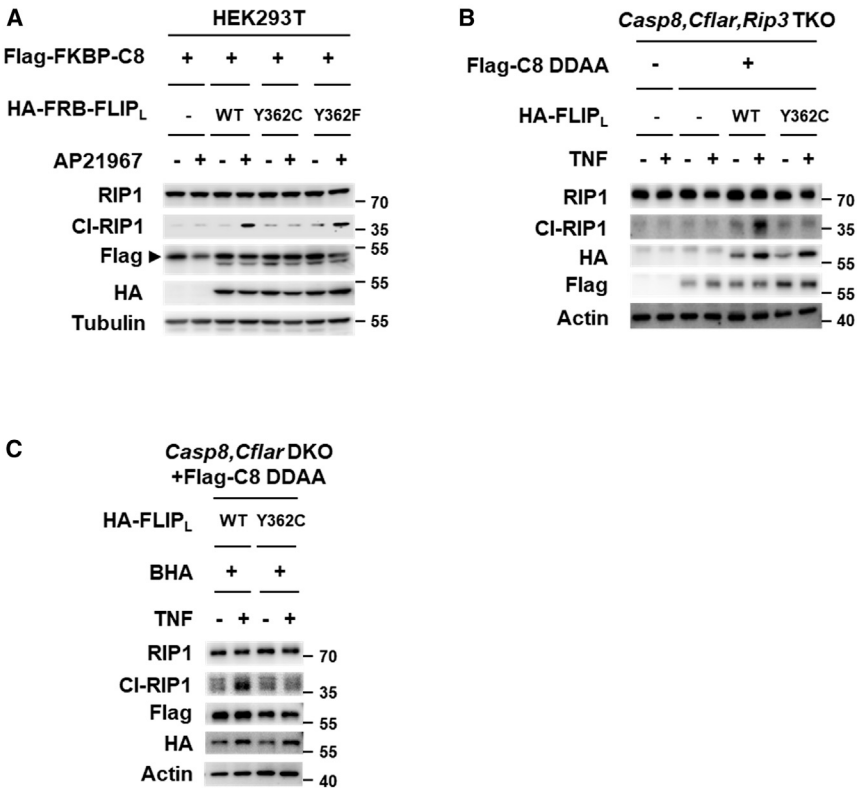

Figure 6. Residue Y362 of $FLIP_L$ is crucial for C8-$FLIP_L$-heterodimer-mediated RIP1 cleavage

(A) The DED domains of caspase-8 (C8)/$FLIP_L$ were substituted with FKBP/FRB domains, respectively. The resulting FKBP-C8/FRB-$FLIP_L$ were transfected in HEK293T cells, as indicated, for 12 h. Then, the cells were treated with AP21967 (500 nM) for 3 h to induce the formation of a heterodimer between FKBP-C8 and FRB-$FLIP_L$. The cell lysates were analyzed by immunoblotting as indicated.

(B) *Casp8*, *Cflar, Rip3* triple knockout (TKO) L929 cells reconstituted with FLAG-C8 DDAA and HA-$FLIP_L$ WT/Y362C were treated with TNF for 3 h. The cell lysates were analyzed by immunoblotting as indicated.

(C) *Casp8*, *Cflar* DKO L929 cells reconstituted with FLAG-C8 DDAA and HA-$FLIP_L$ WT/Y362C were treated with TNF in the presence of BHA (500 μM) for 2 h. The cell lysates were analyzed by immunoblotting as indicated.

All results are representative of at least two independent experiments.

$FLIP_L$(Y362C). To address this issue, we tried to boost the protein expression level of $FLIP_L$(Y362C) in the mutant mouse by using doxycycline (Dox)-induced Tet-On system (Figure S5E). The Tet-On system is basically composed of a transactivator, rtTA (reverse tetracycline-controlled transactivator), and a tetracycline-dependent promotor developed by placing a Tet response element (TRE) upstream of the promoters of genes of interest. In the presence of Dox, the binding of Dox to rtTA will lead to rtTA binding to the TRE and subsequent induced expression of genes of interest. In our system, we inserted a TRE into the site 759 bp upstream of the start codon in the *Cflar* allele in which the Y362C mutation resided to get $Cflar^{+/\text{TRE-Y362C}}$ mice. Then, we crossed $Cflar^{+/\text{TRE-Y362C}}$ mice with $rtTA^{+/-}$ transgenic mice to get $Cflar^{+/\text{TRE-Y362C}}rtTA^{+/-}$ mice. By crossing $Cflar^{+/\text{TRE-Y362C}}rtTA^{+/-}$ mice with $Cflar^{+/\text{TRE-Y362C}}$ mice, we could obtain both $Cflar^{TRE\text{-}Y362C/TRE\text{-}Y362C}$ mice and $Cflar^{TRE\text{-}Y362C/TRE\text{-}Y362C}rtTA^{+/-}$ mice.

We administrated Dox to pregnant surrogate females 1 day after (E1.5) mating $Cflar^{+/\text{TRE-Y362C}}rtTA^{+/-}$ mice with $Cflar^{+/\text{TRE-Y362C}}$ mice by IVF (*in vitro* fertilization). While the expression level of $FLIP_L$ was extremely low in embryos of $Cflar^{TRE\text{-}Y362C/TRE\text{-}Y362C}$ mice, the administration of Dox indeed boosted the expression of $FLIP_L$ in embryos of $Cflar^{TRE\text{-}Y362C/TRE\text{-}Y362C}rtTA^{+/-}$ mice to an extent similar to that in $Cflar^{+/+}rtTA^{+/-}$ mice or $Cflar^{+/+}$ mice (Figure 7A). Consistently, the expression of $FLIP_L$ was barely detected in primary mouse embryonic fibroblasts (MEFs) isolated from $Cflar^{TRE\text{-}Y362C/TRE\text{-}Y362C}rtTA^{+/-}$ mice, and Dox treatment could dramatically increase the expression of $FLIP_L$ (Figure S5F). Timed mating analysis revealed that both $Cflar^{TRE\text{-}Y362C/TRE\text{-}Y362C}$ mice and $Cflar^{TRE\text{-}Y362C/TRE\text{-}Y362C}rtTA^{+/-}$ mice appeared normal at E9.5 (Figure 7B). However, developmental abnormalities beginning around E10.5–E11.5 happened to both $Cflar^{TRE\text{-}Y362C/TRE\text{-}Y362C}$ mice and $Cflar^{TRE\text{-}Y362C/TRE\text{-}Y362C}rtTA^{+/-}$ mice. The vasculature of the yolk sacs of both $Cflar^{TRE\text{-}Y362C/TRE\text{-}Y362C}$ mice and $Cflar^{TRE\text{-}Y362C/TRE\text{-}Y362C}rtTA^{+/-}$ mice showed severe defects, which were observable in embryos or by PECAM-1 staining (Figures 7B, 7D, and 7E). The embryos of both $Cflar^{TRE\text{-}Y362C/TRE\text{-}Y362C}$ mice and $Cflar^{TRE\text{-}Y362C/TRE\text{-}Y362C}rtTA^{+/-}$ mice showed random edema or hemorrhage (Figure 7B). No living embryos of either $Cflar^{TRE\text{-}Y362C/TRE\text{-}Y362C}$ mice or $Cflar^{TRE\text{-}Y362C/TRE\text{-}Y362C}rtTA^{+/-}$ mice were found at E11.5 (Figures 7B and 7C). Immunostaining analysis of the yolk sacs showed that both apoptosis (cleaved caspase-3 [Cl-C3]) and necroptosis (p-MLKL) were increased in $Cflar^{TRE\text{-}Y362C/TRE\text{-}Y362C}rtTA^{+/-}$ mice and $Cflar^{TRE\text{-}Y362C/TRE\text{-}Y362C}$ mice at E10.5 (Figures 7D, 7E, and S5G).

The defects observed in $Cflar^{TRE\text{-}Y362C/TRE\text{-}Y362C}$ mice could result from the lack of sufficient $FLIP_L$ protein, but the defects in $Cflar^{TRE\text{-}Y362C/TRE\text{-}Y362C}rtTA^{+/-}$ mice should reflect the loss of function of $FLIP_L$(Y362C) because the protein level of this $FLIP_L$ mutant was comparable to $FLIP_L$ level in WT mice (Figure 7A). Thus, the function of $FLIP_L$ at E10.5–11.5 is solely to convey pro-caspase-8 activity to cleave RIP1 and perhaps other specific substrates, as the phenotypes of $Cflar^{TRE\text{-}Y362C/TRE\text{-}Y362C}$ and $Cflar^{TRE\text{-}Y362C/TRE\text{-}Y362C}rtTA^{+/-}$ mice are the same. Slightly different from the non-cleavable *Rip1* mutant ($Rip1^{D325A/D325A}$) mice (Figures S5H and S5I),[53–56] $Cflar^{TRE\text{-}Y362C/TRE\text{-}Y362C}rtTA^{+/-}$ mice had more necroptosis (Figure 7E). Altogether, these data demonstrated that the Cys mutation of Y362 in $FLIP_L$ impairs its function in the embryonic development of mice.

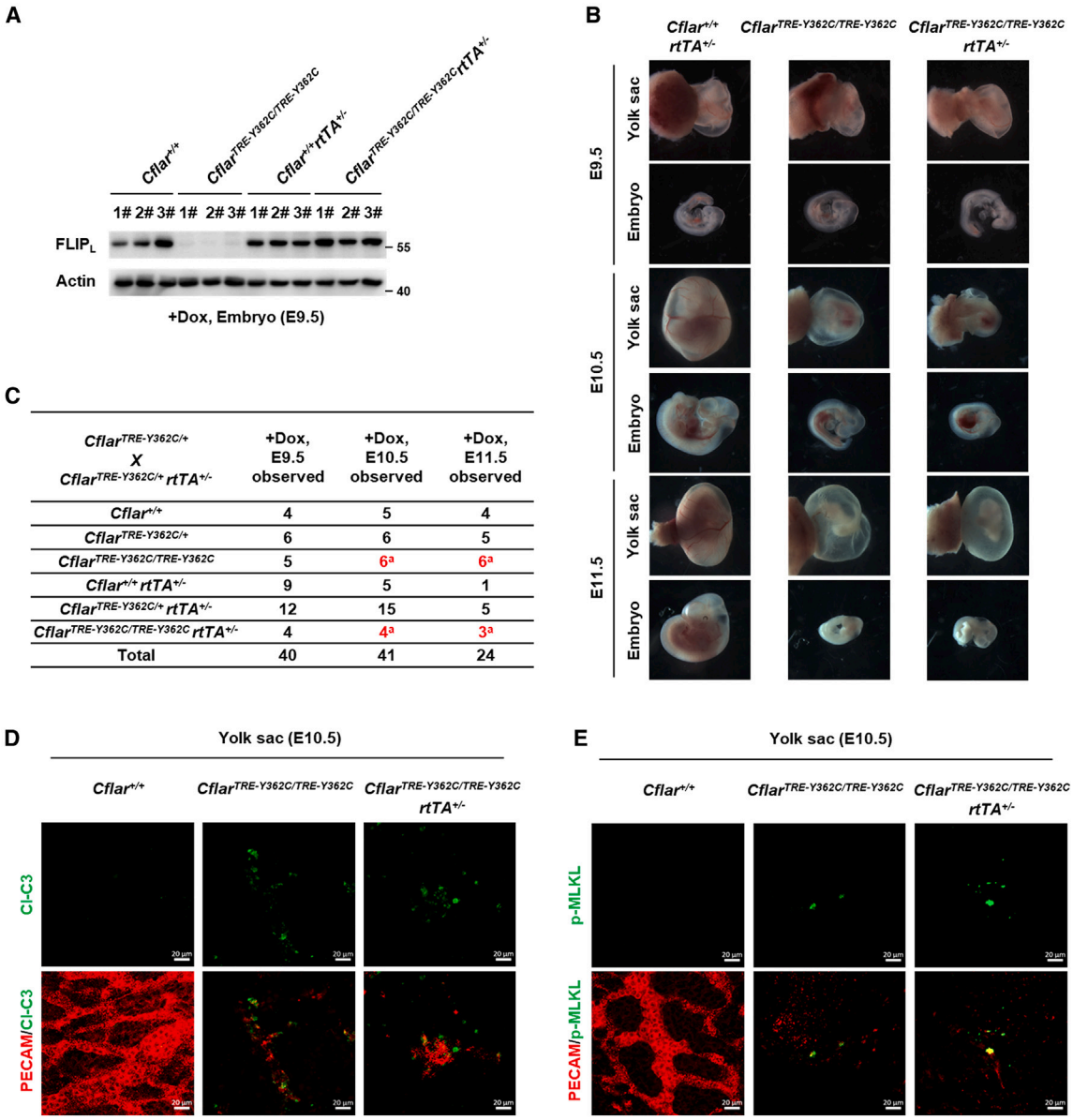

CflarTRE-Y362C/+ X CflarTRE-Y362C/+ rtTA+/-	+Dox, E9.5 observed	+Dox, E10.5 observed	+Dox, E11.5 observed
Cflar+/+	4	5	4
CflarTRE-Y362C/+	6	6	5
CflarTRE-Y362C/TRE-Y362C	5	6[a]	6[a]
Cflar+/+ rtTA+/-	9	5	1
CflarTRE-Y362C/+ rtTA+/-	12	15	5
CflarTRE-Y362C/TRE-Y362C rtTA+/-	4	4[a]	3[a]
Total	40	41	24

Figure 7. Residue Y362 of FLIP$_L$ is indispensable for suppressing necroptosis during the embryonic development of mice

Cflar$^{+/TRE\text{-}Y362C}$*rtTA*$^{+/-}$ mice were crossed with *Cflar*$^{+/TRE\text{-}Y362C}$ mice by IVF (*in vitro* fertilization), and Dox (doxycycline) was administrated to pregnant surrogate females continuously from embryonic day (E)1.5 until the embryos were analyzed.

(A) Immunoblotting analysis for FLIP$_L$ expression in embryos with indicated genotypes at E9.5.

(B) Representative photographs of embryos with indicated genotypes from E9.5 to E11.5. The top shows yolk sacs and the bottom shows side-by-side embryos with yolk sacs removed. Original magnifications, E9.5: ×200, E10.5: ×160, and E11.5: ×125.

(C) Genetic analysis of offspring from E9.5 to E11.5. a, abnormal or dead.

(D) PECAM and cleaved caspase-3 (Cl-C3) staining of yolk sacs with indicated genotypes at E10.5. Scale bar, 20 μm.

(E) PECAM and phospho-MLKL (p-MLKL) staining of yolk sacs with indicated genotypes at E10.5. Scale bar, 20 μm.

All results are representative of at least two independent experiments. See also Figure S5.

DISCUSSION

FLIP$_L$ regulates caspase-8 in two ways: it imparts pro-caspase-8 with activity toward certain substrates such as RIP1 and inhibits pro-caspase-8 maturation.[29,47,69] Currently available data including ours have pointed out that the structural features of FLIP$_L$ empower it to carry out these functions.[35,44–46] It is well accepted that homodimerization of pro-caspase-8 could lead to the trans-autoprocessing and maturation of pro-caspase-8. Because it is a pseudo-protease, FLIP$_L$ cannot cleave pro-caspase-8 to allow its maturation when forming a dimer with it. However, FLIP$_L$-pro-caspase-8 heterodimer retains protease

activity, and we showed here that the structure of $FLIP_L$ is essential for this. $FLIP_L$ and pro-caspase-8 are homologs, but if the Y362 in $FLIP_L$ was converted to Cys (the amino acid in the corresponding position of caspase-8), then $FLIP_L$ would lose its function of conveying pro-caspase-8 to suppress necroptosis. Thus, the input from $FLIP_L$ is required for the protease activity and substrate specificity of the $FLIP_L$-pro-caspase-8 heterodimer. The PL domain in $FLIP_L$ has the function of supporting the protease activity of the $FLIP_L$-pro-caspase-8 heterodimer because the heterodimers of pro-caspase-8 and $FLIP_S$ or other FLIP short variants do not have protease activity toward RIP1.[35,42–46]

The evolutionary origin of caspase-8 can be traced back to porifera (Figure S2C). Before the divergence of Protochordata and Vertebrata, there is only one ancestral *casp8* gene. During the early vertebrate evolution, *casp8*, *cflar*, *casp10*, and *casp18* genes arise from tandem duplication events of the ancestral *casp8* gene. While *casp10* and *casp18* genes are each lost in some specific vertebrate lineages probably due to functional redundancy, *casp8* and *cflar* genes were present in all vertebrate lineages, indicating that both genes are of great importance for organisms.[61–63] As we mentioned earlier, caspase-8 and $FLIP_L$ have the same domain structure, a tandem DED motif domain, and a protease or PL domain. The inhibition of extrinsic apoptosis and necroptosis, respectively, by the activity of the $FLIP_L$-caspase-8 heterodimer is based on data mainly from humans and mice, and whether it is common across all vertebrate species remains to be studied. Previous work found that non-mammalian $FLIP_L$ can function similarly to human $FLIP_L$ in suppressing extrinsic apoptosis in HeLa cells, supporting the idea that the apoptosis-regulating function of $FLIP_L$ is evolutionarily conserved.[61] Thus, one reason for the emergence of $FLIP_L$ may be to control caspase-8-mediated apoptosis. Interestingly, phylogenetic analysis revealed that though the necroptosis executor MLKL arose shortly before vertebrata divergence, other key mediators in the necroptotic axis, including RIP1, TRIF, ZBP1, and RIP3, all appeared right after the divergence of vertebrates.[70–75] As both $FLIP_L$ and core proteins in necroptosis surfaced at the same evolutionary time when vertebrata diverged (Figure S2C), a putative mechanism of coevolution between $FLIP_L$ and necroptosis seems possible. To further investigate this, we examined whether the absence of $FLIP_L$ in genomes coincides with the loss of RIP3 and MLKL, given that RIP3 and MLKL are poorly conserved across vertebrates and each or both are absent in specific clades. For instance, RIP3 is absent in birds and Xenarthra (such as chickens and armadillos), while MLKL is missing in Carnivora within the Mammalia class (such as domestic dogs, domestic cats, and ferrets), and both RIP3 and MLKL are missing in all three sequenced marsupials (such as wallabies, opossums, and Tasmanian devils).[70,72–75] We checked the presence of $FLIP_L$ and caspase-8 in those above-mentioned species by ortholog alignment and found that both $FLIP_L$ and caspase-8 are present and well conserved in all of the aforementioned species. This finding raises two possibilities: one is that $FLIP_L$ may possess multifunction beyond necroptosis regulation, such as apoptosis regulation and caspase-8-independent functions.[33] The other possibility is that although RIP3 and/or MLKL are/is absent in some species, other yet-unidentified proteins may compensate for and contribute to necroptosis fulfillment.[70,72–75] Thus, the lack of a correlated absence of $FLIP_L$ with RIP3 and MLKL loss in specific species cannot exclude the putative mechanism of coevolution between $FLIP_L$ and necroptosis. The evolutionary correlation between $FLIP_L$ and necroptosis remains enigmatic and awaits further exploration.

The anti-cell-death role of $FLIP_L$ made it unneglectable in studying the cell death pathways. FLIP can inhibit a wide range of cell death processes, including those initiated by death receptors and those triggered by clinically relevant chemotherapeutic agents or ionizing radiation. FLIP impacts the survival of both malignant and immune cells.[76] Understanding the structure and function of $FLIP_L$ will provide valuable information for therapeutic inventions of cell-death-related human diseases.

Limitations of the study

Some of our mechanistic interpretations were based on structural modeling rather than real structures. We only provided evidence that the loss-of-function mutation (Y362C) disrupted the structure in the interface between $FLIP_L$ and caspase-8 in computer-generated models, while the silent mutation (Y362F) did not. The modeling certainly has its limitations. The modeled $FLIP_L$(Y362F)-pro-caspase-8 heterodimer structure could be close to the real one because it was not much different from the crystal structure of $FLIP_L$-pro-caspase-8. In contrast, the real structure of the $FLIP_L$(Y362C)-pro-caspase-8 heterodimer may differ from the model. Although the model analyses suggest that a vast structural change was caused by the Y362C mutation in the heterodimer, our modeling cannot reliably predict what kind of structure it changed to. As such, we were unable to interpret why the protein level of $FLIP_L$ was dramatically reduced in Y362C mutant mouse embryos, but this mutation did not influence the half-life of ectopically expressed $FLIP_L$ protein in *Cflar* KO cells. Despite these limitations, our study provides insights into how the structure of $FLIP_L$ imparts caspase-8 unique catalytic activity to block necroptosis independent of $FLIP_L$'s function in suppressing pro-caspase-8 auto-processing. The structure of $FLIP_L$ may coevolve with caspase-8 to tightly keep necroptosis in check.

RESOURCE AVAILABILITY

Lead contact

Further information and requests for resources and reagents should be directed to and will be fulfilled by the lead contact, Zhang-Hua Yang (zhanghuayang@zju.edu.cn).

Materials availability

All plasmids, reagents, cell lines, and mouse lines generated in this study are available from the lead contact.

Data and code availability

- Immunoblot image data and microscopy images reported in this paper will be shared by the lead contact upon request.
- This paper does not report the original code.
- Any additional information required to reanalyze the data reported in this paper is available from the lead contact upon request.

ACKNOWLEDGMENTS

We thank Lu Zhou for help with proofreading and Liang Liu for advice. This work was supported by the National Natural Science Foundation of China

(82388201 to J.H., 32170751 to Z.-H.Y., and 32470864 to X.W.), the National Key R&D Program of China (2020YFA0803500 to J.H.), the Chinese Academy of Medical Sciences (CAMS) Innovation Fund for Medical Science (2019-I2M-5-062 to J.H.), the Fujian Province Central to Local Science and Technology Development Special Program (2022L3079 to J.H.), the Fu-Xia-Quan Zi-Chuang District Cooperation Program (3502ZCQXT2022003 to J.H.), the Leading Innovation and Entrepreneurship Team of Zhejiang Province (2023R01005 to Z.-H.Y.), and the Fundamental Research Funds for the Central Universities (226-2024-00015 to X.W.).

AUTHOR CONTRIBUTIONS

Conceptualization and supervision, J.H. and Z.-H.Y.; data curation, M.H. and X.W., with the help from P.H., R.P., L.L., S.-Q.W., and Y.Z.; formal analysis, M.H., X.W., J.H., and Z.-H.Y.; structure analysis, J.Z. and A.H.; writing – original draft, M.H., J.H., and Z.-H.Y.; writing – review & editing, A.H., J.H., and Z.-H.Y.

DECLARATION OF INTERESTS

The authors declare no competing interests.

STAR★METHODS

Detailed methods are provided in the online version of this paper and include the following:

- KEY RESOURCES TABLE
- EXPERIMENTAL MODEL AND SUBJECT DETAILS
  - Cells
  - Mice
- METHOD DETAILS
  - DNA constructs
  - Lentivirus preparation and infection
  - Treatment
  - Cell viability assay
  - Caspase-8 activity assay
  - Immunoprecipitation and western blotting
  - Timed mating analysis and imaging
  - Immunofluorescence staining and confocal microscopy
  - Quantitative RT-PCR
- QUANTIFICATION AND STATISTICAL ANALYSIS

SUPPLEMENTAL INFORMATION

Supplemental information can be found online at https://doi.org/10.1016/j.celrep.2024.114966.

Received: April 11, 2024
Revised: September 10, 2024
Accepted: October 22, 2024

REFERENCES

1. van Loo, G., and Bertrand, M.J.M. (2023). Death by TNF: a road to inflammation. Nat. Rev. Immunol. *23*, 289–303. https://doi.org/10.1038/s41577-022-00792-3.
2. Ai, Y., Meng, Y., Yan, B., Zhou, Q., and Wang, X. (2024). The biochemical pathways of apoptotic, necroptotic, pyroptotic, and ferroptotic cell death. Mol. Cell. *84*, 170–179. https://doi.org/10.1016/j.molcel.2023.11.040.
3. Yuan, J., and Ofengeim, D. (2024). A guide to cell death pathways. Nat. Rev. Mol. Cell Biol. *25*, 379–395. https://doi.org/10.1038/s41580-023-00689-6.
4. Han, J., Zhong, C.-Q., and Zhang, D.-W. (2011). Programmed necrosis: backup to and competitor with apoptosis in the immune system. Nat. Immunol. *12*, 1143–1149. https://doi.org/10.1038/ni.2159.
5. Pasparakis, M., and Vandenabeele, P. (2015). Necroptosis and its role in inflammation. Nature *517*, 311–320. https://doi.org/10.1038/nature14191.
6. Grootjans, S., Vanden Berghe, T., and Vandenabeele, P. (2017). Initiation and execution mechanisms of necroptosis: an overview. Cell Death Differ. *24*, 1184–1195. https://doi.org/10.1038/cdd.2017.65.
7. Wang, L., Du, F., and Wang, X. (2008). TNF-alpha induces two distinct caspase-8 activation pathways. Cell *133*, 693–703. https://doi.org/10.1016/j.cell.2008.03.036.
8. Zhang, X., Zhang, H., Xu, C., Li, X., Li, M., Wu, X., Pu, W., Zhou, B., Wang, H., Li, D., et al. (2019). Ubiquitination of RIPK1 suppresses programmed cell death by regulating RIPK1 kinase activation during embryogenesis. Nat. Commun. *10*, 4158. https://doi.org/10.1038/s41467-019-11839-w.
9. Tang, Y., Tu, H., Zhang, J., Zhao, X., Wang, Y., Qin, J., and Lin, X. (2019). K63-linked ubiquitination regulates RIPK1 kinase activity to prevent cell death during embryogenesis and inflammation. Nat. Commun. *10*, 4157. https://doi.org/10.1038/s41467-019-12033-8.
10. Gerlach, B., Cordier, S.M., Schmukle, A.C., Emmerich, C.H., Rieser, E., Haas, T.L., Webb, A.I., Rickard, J.A., Anderton, H., Wong, W.W.L., et al. (2011). Linear ubiquitination prevents inflammation and regulates immune signalling. Nature *471*, 591–596. https://doi.org/10.1038/nature09816.
11. Cho, Y.S., Challa, S., Moquin, D., Genga, R., Ray, T.D., Guildford, M., and Chan, F.K.M. (2009). Phosphorylation-driven assembly of the RIP1-RIP3 complex regulates programmed necrosis and virus-induced inflammation. Cell *137*, 1112–1123. https://doi.org/10.1016/j.cell.2009.05.037.
12. He, S., Wang, L., Miao, L., Wang, T., Du, F., Zhao, L., and Wang, X. (2009). Receptor interacting protein kinase-3 determines cellular necrotic response to TNF-alpha. Cell *137*, 1100–1111. https://doi.org/10.1016/j.cell.2009.05.021.
13. Zhang, D.W., Shao, J., Lin, J., Zhang, N., Lu, B.J., Lin, S.C., Dong, M.Q., and Han, J. (2009). RIP3, an energy metabolism regulator that switches TNF-induced cell death from apoptosis to necrosis. Science *325*, 332–336. https://doi.org/10.1126/science.1172308.
14. Li, J., McQuade, T., Siemer, A.B., Napetschnig, J., Moriwaki, K., Hsiao, Y.S., Damko, E., Moquin, D., Walz, T., McDermott, A., et al. (2012). The RIP1/RIP3 necrosome forms a functional amyloid signaling complex required for programmed necrosis. Cell *150*, 339–350. https://doi.org/10.1016/j.cell.2012.06.019.
15. Sun, L., Wang, H., Wang, Z., He, S., Chen, S., Liao, D., Wang, L., Yan, J., Liu, W., Lei, X., and Wang, X. (2012). Mixed lineage kinase domain-like protein mediates necrosis signaling downstream of RIP3 kinase. Cell *148*, 213–227. https://doi.org/10.1016/j.cell.2011.11.031.
16. Zhao, J., Jitkaew, S., Cai, Z., Choksi, S., Li, Q., Luo, J., and Liu, Z.G. (2012). Mixed lineage kinase domain-like is a key receptor interacting protein 3 downstream component of TNF-induced necrosis. Proc. Natl. Acad. Sci. USA *109*, 5322–5327. https://doi.org/10.1073/pnas.1200012109.
17. Cai, Z., Jitkaew, S., Zhao, J., Chiang, H.C., Choksi, S., Liu, J., Ward, Y., Wu, L.G., and Liu, Z.G. (2014). Plasma membrane translocation of trimerized MLKL protein is required for TNF-induced necroptosis. Nat. Cell Biol. *16*, 55–65. https://doi.org/10.1038/ncb2883.
18. Chen, X., Li, W., Ren, J., Huang, D., He, W.T., Song, Y., Yang, C., Li, W., Zheng, X., Chen, P., and Han, J. (2014). Translocation of mixed lineage kinase domain-like protein to plasma membrane leads to necrotic cell death. Cell Res. *24*, 105–121. https://doi.org/10.1038/cr.2013.171.
19. Dondelinger, Y., Declercq, W., Montessuit, S., Roelandt, R., Goncalves, A., Bruggeman, I., Hulpiau, P., Weber, K., Sehon, C.A., Marquis, R.W., et al. (2014). MLKL compromises plasma membrane integrity by binding to phosphatidylinositol phosphates. Cell Rep. *7*, 971–981. https://doi.org/10.1016/j.celrep.2014.04.026.
20. Wang, H., Sun, L., Su, L., Rizo, J., Liu, L., Wang, L.F., Wang, F.S., and Wang, X. (2014). Mixed lineage kinase domain-like protein MLKL causes

necrotic membrane disruption upon phosphorylation by RIP3. Mol. Cell. *54*, 133–146. https://doi.org/10.1016/j.molcel.2014.03.003.

21. Murphy, J.M., Czabotar, P.E., Hildebrand, J.M., Lucet, I.S., Zhang, J.G., Alvarez-Diaz, S., Lewis, R., Lalaoui, N., Metcalf, D., Webb, A.I., et al. (2013). The pseudokinase MLKL mediates necroptosis via a molecular switch mechanism. Immunity *39*, 443–453. https://doi.org/10.1016/j.immuni.2013.06.018.
22. Hildebrand, J.M., Tanzer, M.C., Lucet, I.S., Young, S.N., Spall, S.K., Sharma, P., Pierotti, C., Garnier, J.M., Dobson, R.C.J., Webb, A.I., et al. (2014). Activation of the pseudokinase MLKL unleashes the four-helix bundle domain to induce membrane localization and necroptotic cell death. Proc. Natl. Acad. Sci. USA *111*, 15072–15077. https://doi.org/10.1073/pnas.1408987111.
23. Huyghe, J., Priem, D., and Bertrand, M.J.M. (2023). Cell death checkpoints in the TNF pathway. Trends Immunol. *44*, 628–643. https://doi.org/10.1016/j.it.2023.05.007.
24. Silke, J., Rickard, J.A., and Gerlic, M. (2015). The diverse role of RIP kinases in necroptosis and inflammation. Nat. Immunol. *16*, 689–697. https://doi.org/10.1038/ni.3206.
25. Degterev, A., Huang, Z., Boyce, M., Li, Y., Jagtap, P., Mizushima, N., Cuny, G.D., Mitchison, T.J., Moskowitz, M.A., and Yuan, J. (2005). Chemical inhibitor of nonapoptotic cell death with therapeutic potential for ischemic brain injury. Nat. Chem. Biol. *1*, 112–119. https://doi.org/10.1038/nchembio711.
26. Holler, N., Zaru, R., Micheau, O., Thome, M., Attinger, A., Valitutti, S., Bodmer, J.L., Schneider, P., Seed, B., and Tschopp, J. (2000). Fas triggers an alternative, caspase-8-independent cell death pathway using the kinase RIP as effector molecule. Nat. Immunol. *1*, 489–495. https://doi.org/10.1038/82732.
27. Yang, Z.H., Wu, X.N., He, P., Wang, X., Wu, J., Ai, T., Zhong, C.Q., Wu, X., Cong, Y., Zhu, R., et al. (2020). A Non-canonical PDK1-RSK Signal Diminishes Pro-caspase-8-Mediated Necroptosis Blockade. Mol. Cell. *80*, 296–310.e6. https://doi.org/10.1016/j.molcel.2020.09.004.
28. Kaiser, W.J., Upton, J.W., Long, A.B., Livingston-Rosanoff, D., Daley-Bauer, L.P., Hakem, R., Caspary, T., and Mocarski, E.S. (2011). RIP3 mediates the embryonic lethality of caspase-8-deficient mice. Nature *471*, 368–372. https://doi.org/10.1038/nature09857.
29. Oberst, A., Dillon, C.P., Weinlich, R., McCormick, L.L., Fitzgerald, P., Pop, C., Hakem, R., Salvesen, G.S., and Green, D.R. (2011). Catalytic activity of the caspase-8-FLIP(L) complex inhibits RIPK3-dependent necrosis. Nature *471*, 363–367. https://doi.org/10.1038/nature09852.
30. Alvarez-Diaz, S., Dillon, C.P., Lalaoui, N., Tanzer, M.C., Rodriguez, D.A., Lin, A., Lebois, M., Hakem, R., Josefsson, E.C., O'Reilly, L.A., et al. (2016). The Pseudokinase MLKL and the Kinase RIPK3 Have Distinct Roles in Autoimmune Disease Caused by Loss of Death-Receptor-Induced Apoptosis. Immunity *45*, 513–526. https://doi.org/10.1016/j.immuni.2016.07.016.
31. Zhang, H., Zhou, X., McQuade, T., Li, J., Chan, F.K.M., and Zhang, J. (2011). Functional complementation between FADD and RIP1 in embryos and lymphocytes. Nature *471*, 373–376. https://doi.org/10.1038/nature09878.
32. Green, D.R., Oberst, A., Dillon, C.P., Weinlich, R., and Salvesen, G.S. (2011). RIPK-dependent necrosis and its regulation by caspases: a mystery in five acts. Mol. Cell. *44*, 9–16. https://doi.org/10.1016/j.molcel.2011.09.003.
33. Smyth, P., Sessler, T., Scott, C.J., and Longley, D.B. (2020). FLIP(L): the pseudo-caspase. FEBS J. *287*, 4246–4260. https://doi.org/10.1111/febs.15260.
34. Tsuchiya, Y., Nakabayashi, O., and Nakano, H. (2015). FLIP the Switch: Regulation of Apoptosis and Necroptosis by cFLIP. Int. J. Mol. Sci. *16*, 30321–30341. https://doi.org/10.3390/ijms161226232.
35. Hughes, M.A., Powley, I.R., Jukes-Jones, R., Horn, S., Feoktistova, M., Fairall, L., Schwabe, J.W.R., Leverkus, M., Cain, K., and MacFarlane, M. (2016). Co-operative and Hierarchical Binding of c-FLIP and Caspase-8: A Unified Model Defines How c-FLIP Isoforms Differentially Control Cell Fate. Mol. Cell. *61*, 834–849. https://doi.org/10.1016/j.molcel.2016.02.023.
36. Humphreys, L.M., Fox, J.P., Higgins, C.A., Majkut, J., Sessler, T., McLaughlin, K., McCann, C., Roberts, J.Z., Crawford, N.T., McDade, S.S., et al. (2020). A revised model of TRAIL-R2 DISC assembly explains how FLIP(L) can inhibit or promote apoptosis. EMBO Rep. *21*, e49254. https://doi.org/10.15252/embr.201949254.
37. Irmler, M., Thome, M., Hahne, M., Schneider, P., Hofmann, K., Steiner, V., Bodmer, J.L., Schröter, M., Burns, K., Mattmann, C., et al. (1997). Inhibition of death receptor signals by cellular FLIP. Nature *388*, 190–195. https://doi.org/10.1038/40657.
38. Scaffidi, C., Schmitz, I., Krammer, P.H., and Peter, M.E. (1999). The role of c-FLIP in modulation of CD95-induced apoptosis. J. Biol. Chem. *274*, 1541–1548. https://doi.org/10.1074/jbc.274.3.1541.
39. Krueger, A., Schmitz, I., Baumann, S., Krammer, P.H., and Kirchhoff, S. (2001). Cellular FLICE-inhibitory protein splice variants inhibit different steps of caspase-8 activation at the CD95 death-inducing signaling complex. J. Biol. Chem. *276*, 20633–20640. https://doi.org/10.1074/jbc.M101780200.
40. Fricker, N., Beaudouin, J., Richter, P., Eils, R., Krammer, P.H., and Lavrik, I.N. (2010). Model-based dissection of CD95 signaling dynamics reveals both a pro- and antiapoptotic role of c-FLIPL. J. Cell Biol. *190*, 377–389. https://doi.org/10.1083/jcb.201002060.
41. Kavuri, S.M., Geserick, P., Berg, D., Dimitrova, D.P., Feoktistova, M., Siegmund, D., Gollnick, H., Neumann, M., Wajant, H., and Leverkus, M. (2011). Cellular FLICE-inhibitory protein (cFLIP) isoforms block CD95- and TRAIL death receptor-induced gene induction irrespective of processing of caspase-8 or cFLIP in the death-inducing signaling complex. J. Biol. Chem. *286*, 16631–16646. https://doi.org/10.1074/jbc.M110.148585.
42. Pop, C., Oberst, A., Drag, M., Van Raam, B.J., Riedl, S.J., Green, D.R., and Salvesen, G.S. (2011). FLIP(L) induces caspase 8 activity in the absence of interdomain caspase 8 cleavage and alters substrate specificity. Biochem. J. *433*, 447–457. https://doi.org/10.1042/bj20101738.
43. Boatright, K.M., Deis, C., Denault, J.B., Sutherlin, D.P., and Salvesen, G.S. (2004). Activation of caspases-8 and -10 by FLIP(L). Biochem. J. *382*, 651–657. https://doi.org/10.1042/bj20040809.
44. Yu, J.W., Jeffrey, P.D., and Shi, Y. (2009). Mechanism of procaspase-8 activation by c-FLIPL. Proc. Natl. Acad. Sci. USA *106*, 8169–8174. https://doi.org/10.1073/pnas.0812453106.
45. Micheau, O., Thome, M., Schneider, P., Holler, N., Tschopp, J., Nicholson, D.W., Briand, C., and Grütter, M.G. (2002). The long form of FLIP is an activator of caspase-8 at the Fas death-inducing signaling complex. J. Biol. Chem. *277*, 45162–45171. https://doi.org/10.1074/jbc.M206882200.
46. Chang, D.W., Xing, Z., Pan, Y., Algeciras-Schimnich, A., Barnhart, B.C., Yaish-Ohad, S., Peter, M.E., and Yang, X. (2002). c-FLIP(L) is a dual function regulator for caspase-8 activation and CD95-mediated apoptosis. EMBO J. *21*, 3704–3714. https://doi.org/10.1093/emboj/cdf356.
47. Tummers, B., and Green, D.R. (2017). Caspase-8: regulating life and death. Immunol. Rev. *277*, 76–89. https://doi.org/10.1111/imr.12541.
48. Yeh, W.C., Itie, A., Elia, A.J., Ng, M., Shu, H.B., Wakeham, A., Mirtsos, C., Suzuki, N., Bonnard, M., Goeddel, D.V., and Mak, T.W. (2000). Requirement for Casper (c-FLIP) in regulation of death receptor-induced apoptosis and embryonic development. Immunity *12*, 633–642. https://doi.org/10.1016/s1074-7613(00)80214-9.
49. Dillon, C.P., Oberst, A., Weinlich, R., Janke, L.J., Kang, T.B., Ben-Moshe, T., Mak, T.W., Wallach, D., and Green, D.R. (2012). Survival function of the FADD-CASPASE-8-cFLIP(L) complex. Cell Rep. *1*, 401–407. https://doi.org/10.1016/j.celrep.2012.03.010.
50. Zhang, H., Rosenberg, S., Coffey, F.J., He, Y.W., Manser, T., Hardy, R.R., and Zhang, J. (2009). A role for cFLIP in B cell proliferation and stress

MAPK regulation. J. Immunol. *182*, 207–215. https://doi.org/10.4049/jimmunol.182.1.207.

51. Piao, X., Komazawa-Sakon, S., Nishina, T., Koike, M., Piao, J.H., Ehlken, H., Kurihara, H., Hara, M., Van Rooijen, N., Schütz, G., et al. (2012). c-FLIP maintains tissue homeostasis by preventing apoptosis and programmed necrosis. Sci. Signal. *5*, ra93. https://doi.org/10.1126/scisignal.2003558.
52. Oberst, A., and Green, D.R. (2011). It cuts both ways: reconciling the dual roles of caspase 8 in cell death and survival. Nat. Rev. Mol. Cell Biol. *12*, 757–763. https://doi.org/10.1038/nrm3214.
53. Newton, K., Wickliffe, K.E., Dugger, D.L., Maltzman, A., Roose-Girma, M., Dohse, M., Kőműves, L., Webster, J.D., and Dixit, V.M. (2019). Cleavage of RIPK1 by caspase-8 is crucial for limiting apoptosis and necroptosis. Nature *574*, 428–431. https://doi.org/10.1038/s41586-019-1548-x.
54. Zhang, X., Dowling, J.P., and Zhang, J. (2019). RIPK1 can mediate apoptosis in addition to necroptosis during embryonic development. Cell Death Dis. *10*, 245. https://doi.org/10.1038/s41419-019-1490-8.
55. Lalaoui, N., Boyden, S.E., Oda, H., Wood, G.M., Stone, D.L., Chau, D., Liu, L., Stoffels, M., Kratina, T., Lawlor, K.E., et al. (2020). Mutations that prevent caspase cleavage of RIPK1 cause autoinflammatory disease. Nature *577*, 103–108. https://doi.org/10.1038/s41586-019-1828-5.
56. Zhang, Y., Huang, K., Zhang, Y., Han, T., Li, L., Ruan, C., Sun, Y.H., Shi, W., Han, W., Wu, S.Q., et al. (2021). A unique death pathway keeps RIPK1 D325A mutant mice in check at embryonic day 10.5. PLoS Biol. *19*, e3001304. https://doi.org/10.1371/journal.pbio.3001304.
57. Vercammen, D., Vandenabeele, P., Beyaert, R., Declercq, W., and Fiers, W. (1997). Tumour necrosis factor-induced necrosis versus anti-Fas-induced apoptosis in L929 cells. Cytokine *9*, 801–808. https://doi.org/10.1006/cyto.1997.0252.
58. Vercammen, D., Beyaert, R., Denecker, G., Goossens, V., Van Loo, G., Declercq, W., Grooten, J., Fiers, W., and Vandenabeele, P. (1998). Inhibition of caspases increases the sensitivity of L929 cells to necrosis mediated by tumor necrosis factor. J. Exp. Med. *187*, 1477–1485. https://doi.org/10.1084/jem.187.9.1477.
59. Majkut, J., Sgobba, M., Holohan, C., Crawford, N., Logan, A.E., Kerr, E., Higgins, C.A., Redmond, K.L., Riley, J.S., Stasik, I., et al. (2014). Differential affinity of FLIP and procaspase 8 for FADD's DED binding surfaces regulates DISC assembly. Nat. Commun. *5*, 3350. https://doi.org/10.1038/ncomms4350.
60. Hu, S., Vincenz, C., Ni, J., Gentz, R., and Dixit, V.M. (1997). I-FLICE, a novel inhibitor of tumor necrosis factor receptor-1- and CD-95-induced apoptosis. J. Biol. Chem. *272*, 17255–17257. https://doi.org/10.1074/jbc.272.28.17255.
61. Sakamaki, K., Iwabe, N., Iwata, H., Imai, K., Takagi, C., Chiba, K., Shukunami, C., Tomii, K., and Ueno, N. (2015). Conservation of structure and function in vertebrate c-FLIP proteins despite rapid evolutionary change. Biochem. Biophys. Rep. *3*, 175–189. https://doi.org/10.1016/j.bbrep.2015.08.005.
62. Sakamaki, K., Imai, K., Tomii, K., and Miller, D.J. (2015). Evolutionary analyses of caspase-8 and its paralogs: Deep origins of the apoptotic signaling pathways. Bioessays *37*, 767–776. https://doi.org/10.1002/bies.201500010.
63. Sakata, S.i., Yan, Y., Satou, Y., Momoi, A., Ngo-Hazelett, P., Nozaki, M., Furutani-Seiki, M., Postlethwait, J.H., Yonehara, S., and Sakamaki, K. (2007). Conserved function of caspase-8 in apoptosis during bony fish evolution. Gene *396*, 134–148. https://doi.org/10.1016/j.gene.2007.03.010.
64. Shu, H.B., Halpin, D.R., and Goeddel, D.V. (1997). Casper is a FADD- and caspase-related inducer of apoptosis. Immunity *6*, 751–763. https://doi.org/10.1016/s1074-7613(00)80450-1.
65. Xu, J.H., Eberhardt, J., Hill-Payne, B., González-Páez, G.E., Castellón, J.O., Cravatt, B.F., Forli, S., Wolan, D.W., and Backus, K.M. (2020). Integrative X-ray Structure and Molecular Modeling for the Rationalization of Procaspase-8 Inhibitor Potency and Selectivity. ACS Chem. Biol. *15*, 575–586. https://doi.org/10.1021/acschembio.0c00019.
66. Thompson, B., and Petrić Howe, N. (2024). Alphafold 3.0: the AI protein predictor gets an upgrade. Nature. https://doi.org/10.1038/d41586-024-01385-x.
67. Tao, P., Sun, J., Wu, Z., Wang, S., Wang, J., Li, W., Pan, H., Bai, R., Zhang, J., Wang, Y., et al. (2020). A dominant autoinflammatory disease caused by non-cleavable variants of RIPK1. Nature *577*, 109–114. https://doi.org/10.1038/s41586-019-1830-y.
68. Zhang, Y., Su, S.S., Zhao, S., Yang, Z., Zhong, C.Q., Chen, X., Cai, Q., Yang, Z.H., Huang, D., Wu, R., and Han, J. (2017). RIP1 autophosphorylation is promoted by mitochondrial ROS and is essential for RIP3 recruitment into necrosome. Nat. Commun. *8*, 14329. https://doi.org/10.1038/ncomms14329.
69. Green, D.R. (2022). Nonapoptotic Cell Death Pathways. Cold Spring Harbor Perspect. Biol. *14*, a041079. https://doi.org/10.1101/cshperspect.a041079.
70. Dondelinger, Y., Hulpiau, P., Saeys, Y., Bertrand, M.J.M., and Vandenabeele, P. (2016). An evolutionary perspective on the necroptotic pathway. Trends Cell Biol. *26*, 721–732. https://doi.org/10.1016/j.tcb.2016.06.004.
71. Degterev, A., and Yuan, J. (2008). Expansion and evolution of cell death programmes. Nat. Rev. Mol. Cell Biol. *9*, 378–390. https://doi.org/10.1038/nrm2393.
72. Horne, C.R., Samson, A.L., and Murphy, J.M. (2023). The web of death: the expanding complexity of necroptotic signaling. Trends Cell Biol. *33*, 162–174. https://doi.org/10.1016/j.tcb.2022.05.008.
73. Newton, K., and Manning, G. (2016). Necroptosis and Inflammation. Annu. Rev. Biochem. *85*, 743–763. https://doi.org/10.1146/annurev-biochem-060815-014830.
74. Tummers, B., and Green, D.R. (2022). The evolution of regulated cell death pathways in animals and their evasion by pathogens. Physiol. Rev. *102*, 411–454. https://doi.org/10.1152/physrev.00002.2021.
75. Águeda-Pinto, A., Alves, L.Q., Neves, F., McFadden, G., Jacobs, B.L., Castro, L.F.C., Rahman, M.M., and Esteves, P.J. (2021). Convergent Loss of the Necroptosis Pathway in Disparate Mammalian Lineages Shapes Viruses Countermeasures. Front. Immunol. *12*, 747737. https://doi.org/10.3389/fimmu.2021.747737.
76. Humphreys, L., Espona-Fiedler, M., and Longley, D.B. (2018). FLIP as a therapeutic target in cancer. FEBS J. *285*, 4104–4123. https://doi.org/10.1111/febs.14523.

STAR★METHODS

KEY RESOURCES TABLE

REAGENT or RESOURCE	SOURCE	IDENTIFIER
Antibodies		
Rabbit anti-Flag	Cell Signaling Technology	Cat#14793; RRID:AB_2572291
Rabbit anti-FLIP	Cell Signaling Technology	Cat#56343; RRID:AB_2799508
Rabbit anti-RIP1	Cell Signaling Technology	Cat#3493; RRID:AB_2305314
Rabbit anti-caspase-8	Cell Signaling Technology	Cat#4790; RRID:AB_10545768
Rabbit anti-cleaved-caspase-8 (p43 & p18)	Cell Signaling Technology	Cat#9429; RRID:AB_2068300
Rabbit anti-HA (Y-11)	Santa Cruz Biotechnology	Cat#sc-805; RRID:AB_631618
Mouse anti-β-actin (C4)	Santa Cruz Biotechnology	Cat#sc-47778; RRID:AB_626632
Rabbit anti-phospho-RIP3 (T231, S232)	Abcam	Cat#ab222320; RRID:AB_2868434
Rabbit anti-phospho-MLKL (S345)	Abcam	Cat#ab196436; RRID:AB_2687465
Rabbit anti-RIP3	ProSci	Cat#2283; RRID:AB_203256
Rabbit anti-MLKL	Proteintech	Cat#66675-1-Ig; RRID:AB_2882029
Rabbit anti-FADD	Yang et al.[27]	N/A
Rat anti-PECAM (CD31)	BD Biosciences	Cat#550274; RRID:AB_393571
Rabbit anti-cleaved-caspase-3 (p19 & 17)	Cell Signaling Technology	Cat#9661; RRID:AB_2341188
Alexa Fluor 594 goat anti-rat antibody	Invitrogen	Cat#A11007; RRID:AB_10561522
Alexa Fluor 488 goat anti-rabbit antibody	Invitrogen	Cat#A11034; RRID:AB_2576217
Chemicals, peptides, and recombinant proteins		
Murine TNFα	Thermo Fisher	Cat#PMC3015
Z-VAD-FMK	Calbiochem	Cat#627610
Necrostatin-1 (Nec-1)	EMD Chemicals	Cat#480065
Z-DEVD-FMK	MCE	Cat#HY-12466
Doxycycline hyclate	MCE	Cat#HY-N0565B
AP21967 (now A/C Heterodimerizer)	Takara	Cat#635057
Butylated hydroxyanisole (BHA)	Sigma	Cat#B1253-5G
Polybrene	Sigma-Aldrich	Cat#H9268
Propidium iodide (PI)	Sigma-Aldrich	Cat#P4170
Cycloheximide (CHX)	Sigma-Aldrich	Cat#C7698
Lambda protein phosphatase	Beyotime	Cat#P2316S
Critical commercial assays		
CellTiter-Glo® Luminescent Cell Viability Assay	Promega	Cat#G7571
Caspase-Glo® 8 Assay	Promega	Cat#G8202
Experimental models: Cell lines		
Human: (HEK) 293T	ATCC	Cat#CRL-3216
Mouse: L929 cells	Zhang et al.[13]	N/A
Mouse: Mouse embryonic fibroblasts (MEFs)	This paper	N/A
Mouse: Bone marrow-derived macrophages (BMDMs)	This paper	N/A
Mouse: Intestinal epithelial cells (IECs)	This paper	N/A
Experimental models: Organisms/strains		
C57BL/6J	Jackson Laboratory	000664
Cflar$^{+/Y362C}$ and *Cflar*$^{+/TRE\text{-}Y362C}$ mice	This paper	N/A
CMV^{CRE} mice	Jackson Laboratory	006054
rtTA^{flox} mice	Jackson Laboratory	005670

(*Continued on next page*)

Continued

REAGENT or RESOURCE	SOURCE	IDENTIFIER
Oligonucleotides		
sgRNA was designed to target *Cflar* for *Cflar* KO L929 cells: 5′-GTCTGCCGAGGTCATTCACC-3′	This paper	N/A
sgRNA was designed to target *Casp8* for *Casp8* KO L929 cells: 5′-GGTCTAGGAAGTTGACCAGC-3′	This paper	N/A
TALENs′ target sites on mouse *Rip3*: (Left) 5′-CTAACATTCTGCTGGA-3′	This paper	N/A
TALENs′ target sites on mouse *Rip3*: (Right) 5′-TGTAGATGGACTAACC-3′	This paper	N/A
sgRNA was designed to target *Cflar* for $Cflar^{+/Y362C}$ mice: 5′-ATTCAGAACTATGAGTCGTT-3′	This paper	N/A
sgRNA was designed to target *Cflar* for $Cflar^{+/TRE\text{-}Y362C}$ mice: 5′-ATGGCCATTGCTGCCGTGGG-3′	This paper	N/A
RT-PCR primers for mouse *Cflar* (Forward): 5′-GCTCCAGAATGGGCGAAGTAA-3′;	This paper	N/A
RT-PCR primers for mouse *Cflar* (Reverse): 5′-ACGGATGTGCGGAGGTAAAAA-3′	This paper	N/A
RT-PCR primers for mouse *Gapdh* (Forward): 5′-ATGGTGAAGGTCGGTGTGAAC-3′;	This paper	N/A
RT-PCR primers for mouse *Gapdh* (Reverse): 5′-GTCAGTGCGAGGCTGTGATG-3′	This paper	N/A
Recombinant DNA		
pBOBI-Flag-Caspase-8 WT	This paper	N/A
pBOBI-Flag-Caspase-8 C362S	This paper	N/A
pBOBI-Flag-Caspase-8 DDAA (D218A + D387A)	This paper	N/A
pBOBI-HA-Caspase-8 C362Y	This paper	N/A
pBOBI-HA-$FLIP_L$ WT	This paper	N/A
pBOBI-HA-$FLIP_L$ ΔDED1	This paper	N/A
pBOBI-HA-$FLIP_L$ ΔDED2	This paper	N/A
pBOBI-HA-$FLIP_L$ ΔDED1&2	This paper	N/A
pBOBI-HA-$FLIP_L$ ΔPL	This paper	N/A
pBOBI-HA-$FLIP_L$ L317H + Y362C	This paper	N/A
pBOBI-HA-$FLIP_L$ L317H	This paper	N/A
pBOBI-HA-$FLIP_L$ Y362C	This paper	N/A
pBOBI-HA-$FLIP_L$ Y362F	This paper	N/A
pBOBI-HA-$FLIP_L$ G318A	This paper	N/A
pBOBI-HA-$FLIP_L$ Q360A	This paper	N/A
pBOBI-HA-$FLIP_L$ K416A	This paper	N/A
pBOBI-HA-$FLIP_L$ S422A	This paper	N/A
pBOBI-HA-$FLIP_L$ 4A (G318A + Q360A + K416A + S422A)	This paper	N/A
pBOBI-Flag-FKBP-Caspase-8 ΔDED	This paper	N/A
pBOBI-HA-FRB-$FLIP_L$ ΔDED	This paper	N/A
Software and algorithms		
GraphPad Prism 6.01	GraphPad	https://www.graphpad.com/scientific-software/prism/
BioRender	BioRender	https://biorender.com

(*Continued on next page*)

Continued

REAGENT or RESOURCE	SOURCE	IDENTIFIER
Aperio ImageScope 64 v12.4.0.5043	Leica	https://www.leicabiosystems.com/cn/digital-pathology/manage/aperio-imagescope/
ZEN (blue edition)	ZEISS	https://www.zeiss.com.cn/microscopy/products/microscope-software/zen.html
Other		
Flag-M2 affinity resin	Sigma-Aldrich	Cat#A2220
Anti-HA Affinity Gel	Beyotime	Cat#P2287
Protease Inhibitor Cocktail	Sigma-Aldrich	Cat#S8820
FACS Calibur flow cytometer	BD Bioscience	https://www.bdbiosciences.com/en-us
POLAR star Omega	BMG Labtech	https://www.bmglabtech.com/cn/polarstar-omega/

EXPERIMENTAL MODEL AND SUBJECT DETAILS

Cells

Human embryonic kidney (HEK) 293T cells and mouse fibroblast L929 cells were obtained from the American Type Culture Collection (ATCC) (Manassas, VA, USA). *Cflar* KO, *Casp8* KO, *Casp8*, *Cflar* DKO and *Casp8*, *Cflar, Rip3* TKO L929 cell lines were generated using CRISPR/Cas9 method and TALE-nuclease (TALENs) method. The target sequences in the gRNA vector were 5′-GTC TGCCGAGGTCATTCACC-3′ for mouse *Cflar*, 5′-GGTCTAGGAAGTTGACCAGC-3′ for mouse *Casp8*. TALENs' target sites for mouse *Rip3* were 5′-CTAACATTCTGCTGGA-3' (Left) and 5′-TGTAGATGGACTAACC-3' (Right). The disruption of the target gene was determined by the sequencing of gene loci and by the immunoblotting of cell lysates with antibodies. HEK293T cells and L929 cells were cultured in Dulbecco's Modified Eagle's Medium (DMEM) (Invitrogen) supplemented with 10% (v/v) fetal bovine serum (FBS) (GIBCO), 1% (v/v) MEM non-essential amino acids solution (Hyclone), 100 units/ml penicillin/streptomycin, at 37°C in a humidified incubator containing 5% CO2. Bone marrow-derived macrophages (BMDMs) were generated by differentiating bone marrow progenitors from the tibia and femur of mice for 7 days in DMEM supplemented with 10% (v/v) heat-inactivated FBS and 30% (v/v) L929-conditioned medium and were grown at 37°C in a 5% CO2 incubator. Intestinal epithelial cells (IECs) were separated from the cut cecum fragment of mice by EDTA (5 mM) digestion (at 37°C for 1 h) and single cell isolation (vortex, followed by passing cell suspensions through a cell strainer). After separation, IECs were not cultured and directly used for sample preparation.

Mice

Cflar$^{+/Y362C}$ mice were generated by co-microinjection of *in vitro* transcribed Cas9 mRNA, gRNA and homologous-recombination template oligo into the C57BL/6J zygotes. The target sequence in the gRNA vector was 5′-ATTCAGAACTATGAGTCGTT-3′ for mouse *Cflar* Y362C mutation. *Cflar*$^{+/Y362C}$ mice were validated by genomic fragment sequencing. *Cflar*$^{+/TRE\text{-}Y362C}$ mice were generated by co-microinjection of *in vitro* transcribed Cas9 mRNA, gRNA and homologous-recombination template plasmid containing a Tet Response Element (TRE) sequence into the *Cflar*$^{+/Y362C}$ zygotes. The target sequence in the gRNA vector was 5′-ATGGCC ATTGCTGCCGTGGG-3′ for TRE insertion. *Cflar*$^{+/TRE\text{-}Y362C}$ mice were validated by genomic fragment sequencing and crossing with C57BL/6J wildtype mice to make sure that the TRE was inserted into the site 759bp upstream of the start codon in *Cflar* allele where Y362C mutation resided. *rtTA*$^{+/-}$ transgenic mice, in which rtTA (reverse tetracycline-controlled transactivator) was constitutively expressed, were developed by crossing *CMV*^{cre} mice (Jax stock, 006054) with *rtTA*^{flox} mice (Jax stock, 005670). All mice were in the C57BL/6J background. Additional information is provided upon request. All mice were housed in specific pathogen-free condition with 12-h light/dark cycle and access to food and water *ad libitum* at the Xiamen University Laboratory Animal Center. All mouse experiments were approved by the Institutional Animal Care and Use Committee and were in strict accordance with good animal practice as defined by the Xiamen University Laboratory Animal Center.

METHOD DETAILS

DNA constructs

Wildtype (WT) full-lengths of mouse $FLIP_L$ and mouse caspase-8 were amplified from a cDNA library derived from L929 cells. $FLIP_L$ mutations (L317H + Y362C, L317H, Y362C, Y362F, G318A, Q360A, K416A, S422A and 4A(G318A+Q360A+K416A+S422A)) and caspase-8 mutations (C362S, C362Y and DDAA(D218A + D387A)) were introduced by two-round PCR. $FLIP_L$ truncations ($FLIP_L$ ΔDED and $FLIP_L$ ΔPL) were introduced by standard PCR using its WT full-length template. To generate fusion proteins, FKBP,

FRB* (T2098L), protease domain of caspase-8, and protease-like domain of $FLIP_L$ (WT/Y362F/Y362C) were amplified by standard PCR from the corresponding templates. All of these DNA fragments were cloned into the lentiviral vector pBOBI containing Flag/HA tags using the Exo III-assisted ligase-free cloning method. All plasmids were verified by DNA sequencing.

Lentivirus preparation and infection

HEK293T cells were co-transfected with pBOBI constructs and lentivirus-packing plasmids (PMDL/REV/VSVG) by the calcium phosphate precipitation method. 12 h later, cell culture medium was changed and the virus-containing medium was collected 36 h later. For infection, virus containing medium in the presence of 10 μg/mL Polybrene was added to cells plated in 12-well plates and then centrifuged at 2,500 rpm for 30 min. The medium was changed 12 h later.

Treatment

Cells were treated with mouse TNF (10 ng/mL), zVAD (20 μM), Nec-1 (30 μM), DEVD (20 μM), AP21967 (500 nM), and BHA (500 μM). Pre-treatment was performed 30 min ahead. When needed, pregnant surrogate female mice were treated with 2 mg/mL Dox plus 5% (w/v) sucrose in drinking water.

Cell viability assay

Cell viability was analyzed using FACS or CellTiter-Glo Luminescent Cell Viability Assay kit (Promega, Madison, WI, USA). FACS analysis was performed as previously described (Zhang et al., 2009). In brief, cells were trypsinized with PBS containing 5 μg/mL Propidium iodide (PI) and quantified on a FACS Calibur flow cytometer. PI-negative cells with normal size were considered living cells. The Luminescent Cell Viability Assays were performed according to the manufacturer's instructions. In brief, 3.0×10^4 cells were seeded in 96-well plates with white wall for 12 h. After treatment, an equal volume of CellTiter-Glo reagent was added to the cell culture medium, which had been equilibrated to room temperature for 30 min. Cells were shaken for 5 min and incubated at room temperature for 15 min. Luminescent recording was performed with POLAR star Omega (BMG Labtech, Durham, NC, USA).

Caspase-8 activity assay

Caspase-8 activity was determined by using Caspase-Glo 8 Assay kit (Promega, Madison, WI, USA) according to the manufacturer's instructions. In brief, 3.0×10^4 cells were seeded in 96-well plates with white for 12 h. After treatment, an equal volume of Caspase-Glo 8 reagent was added to the cell culture medium, which had been equilibrated to room temperature for 30 min. Cells were shaken for 5 min and incubated at room temperature for 30 min. Luminescent recording was performed with POLAR star Omega (BMG Labtech, Durham, NC, USA).

Immunoprecipitation and western blotting

For Flag or HA immunoprecipitation, cells were washed with ice-cold PBS and lysed in lysis buffer (20 mM Tris-HCl, pH7.5, 150 mM NaCl, 1 mM Na_2EDTA, 1 mM EGTA, 1% Triton X-100, 2.5 mM sodium pyrophosphate, 1 mM β-glycerophosphate, 1 mM Na_3VO_4) supplemented with Sigma Protease Inhibitor Cocktail. The cell lysates were centrifuged at 20 000 × g for 30 min, and the supernatants were subjected to immunoprecipitation with mouse anti-Flag M2 beads at 4°C overnight. After the immunoprecipitation, the beads were washed three times with lysis buffer. The immunoprecipitated proteins were eluted and subsequently analyzed by western blotting. Immunoprecipitates, tissue lysates and cell lysates were resolved by SDS-PAGE, transferred onto a polyvinylidene difluoride membrane, and probed with corresponding antibodies.

Timed mating analysis and imaging

For timed mating experiment, 3- to 4-month-old, experienced stud males with specific genotypes were prepared 1 to 2 weeks before mating. Adequate amounts of 4-week-old females with specific genotypes were prepared before mating as well. The mating between stud males and females was conducted by *in vitro* fertilization (IVF) at 11:00 a.m. The next afternoon when the 2-cell zygotes were transplanted into surrogate females was set as embryonic day 0.5 (E0.5). When Dox administration was needed, pregnant surrogate females were treated with 2 mg/mL Dox plus 5% (w/v) sucrose in drinking water continuously from E1.5. At 1:00 p.m. of E10.5 or other embryonic stages as indicated, pregnant surrogate females were killed and embryos were isolated. Images of yolk sacs and embryos with yolk sacs removed were captured on Leica M165FC microscope (Leica Microsystems GmbH, Germany). Then sections of yolk sacs were used for genotyping.

Immunofluorescence staining and confocal microscopy

Yolk sacs were harvested, mounted on adhesion microscope slides (ZSGB-Bio), and fixed for 4 h at 4°C using 4% paraformaldehyde in PBS. Cells were permeabilized for 45 min in 0.25% Triton X-100 in PBS. For Phosphatase treatment, the yolk sacs were further permeabilized for 10 min at room temperature with 0.1% Triton X-100 dissolved in Dulbecco's Phosphate Buffered Saline solution (DPBS) containing $CaCl_2$ and $MgCl_2$. Later, dephosphorylation was carried out using a solution containing: 18 μL of lambda protein phosphatase (PPse) (70,000 units/mL) (Beyotime, Cat. no: P2316S), 15 μL NEBuffer Pack for Protein MetalloPhosphatases (PMP), 15 μL $MnCl_2$ and 467 μL of DPBS ($CaCl_2$ and $MgCl_2$). A total of 500 μL of lambda PPse-containing solution were used per slide. The slides were incubated for 3 h at 30°C. Then the slices were blocked for 1 h in PBS containing 2% goat serum, and then incubated

overnight at 4°C with rabbit anti-cleaved caspase-3 antibody or rabbit anti-phospho-MLKL (S345) antibody along with rat anti-PECAM (CD31) antibody diluted in blocking buffer. Yolk sacs were washed 3 times with PBS and then incubated for 1 h at room temperature with Alexa Fluor 488 goat anti-rabbit antibody and Alexa Fluor 594 goat anti-rat antibody. Images were acquired on a Zeiss LSM 780 laser scanning confocal microscope (Carl Zeiss Microscopy GmbH, Germany).

Quantitative RT-PCR

Total RNA was extracted from BMDMs with RNAiso Plus (Takara) according to the manufacturer's instructions. cDNA was prepared with M-MLV reverse transcriptase and oligo-dT primers. Quantitative RT-PCR was performed using SYBR Green reagent along with gene-specific primers. All the results were analyzed by relative quantification, by normalizing to the *Gapdh* RNA level. Sequences of primers used to detect transcripts of genes were 5′-GCTCCAGAATGGGCGAAGTAA-3′(forward) and 5′-ACGGATGTGCGGAGG TAAAAA-3′(reverse) for mouse *Cflar*, and 5′-ATGGTGAAGGTCGGTGTGAAC-3′(forward) and 5′-GTCAGTGCGAGGCTGTGATG-3′(reverse) for mouse *Gapdh*.

QUANTIFICATION AND STATISTICAL ANALYSIS

No statistical methods were used to predetermine the sample size. GraphPad Prism software was used for data analysis. Data are shown as mean ± standard deviation (SD).